Intelligent and Converged Networks ISSN 2708-6240
2022, 3(1): 86−102 DOI: 10.23919/ICN.2022.0001

User cooperation for IRS-aided secure MIMO systems

(*invited paper*)

Gui Zhou, Cunhua Pan*, Hong Ren, Kezhi Wang, Kok Keong Chai, and Kai-Kit Wong

Abstract: An intelligent reflecting surface (IRS) is proposed to enhance the physical layer security in the Rician fading channel wherein the angular direction of the eavesdropper (ED) is aligned with a legitimate user. A two-phase communication system under active attacks and passive eavesdropping is considered in this scenario. The base station avoids direct transmission to the attacked user in the first phase, whereas other users cooperate in forwarding signals to the attacked user in the second phase, with the help of IRS and energy harvesting technology. Under the occurrence of active attacks, an outage-constrained beamforming design problem is investigated under the statistical cascaded channel error model, which is solved by using the Bernstein-type inequality. An average secrecy rate maximization problem for the passive eavesdropping is formulated, which is then addressed by a low-complexity algorithm. The numerical results of this study reveal that the negative effect of the ED's channel error is larger than that of the legitimate user.

Key words: intelligent reflecting surface (IRS); reconfigurable intelligent surface (RIS); robust design; energy harvesting; physical layer security

1 Introduction

Intelligent reflecting surface (IRS), also known as reconfigurable intelligent surface (RIS), is a planar surface consisting of massive amounts of passive and low-cost reflecting elements. In recent years, the IRS has emerged as a promising technique to reconfigure the wireless propagation environment by imposing phase shifts on the incident electromagnetic signals[2−4]. Based on the exploration of the differences in channel conditions and interference environment, the IRS can change the reflection direction of the incident signal, thus allowing it to enhance the received signals of legitimate users (LUs) while also suppressing the signals received by the eavesdropper (ED)[5−9]. Thus, the IRS has the potential of mitigating the interference, extending the coverage area, and improving the physical layer security communication. Furthermore, the IRS can be readily coated on existing buildings, such as ceilings and walls, which can reduce both the cost and complexity of deployment operations. Hence, the IRS provides a cost-effective and energy-efficient approach, thus holding great promise for security enhancement.

In general, EDs work in two modes: active attacks and passive eavesdropping[10, 11]. In an active attack, the ED misleads the base station (BS) to send signals to the ED by pretending to be an LU sending pilot signals to the BS during the channel estimation procedure. Nonetheless, a passive attack is more challenging to

• Gui Zhou and Kok Keong Chai are with the School of Electronic Engineering and Computer Science, Queen Mary University of London, London, E1 4NS, UK. E-mail: {g.zhou; michael.chai}@qmul.ac.uk.
• Cunhua Pan and Hong Ren are with the National Mobile Communications Research Laboratory, Southeast University, Nanjing 210096, China. E-mail: {cpan; hren}@seu.edu.cn.
• Kezhi Wang is with the Department of Computer and Information Sciences, Northumbria University, Newcastle upon Tyne, NE1 8ST, UK. E-mail: kezhi.wang@northumbria.ac.uk.
• Kai-Kit Wong is with the Department of Electronic and Electrical Engineering, University College London, London, WC1E 6BT, UK. E-mail: kai-kit.wong@ucl.ac.uk.
• Part of this work has been published in Ref. [1].
∗ To whom correspondence should be addressed.
Manuscript received: 2021-11-09; revised: 2021-12-20; accepted: 2022-02-11

tackle because the passive ED can hide itself. Furthermore, its channel state information (CSI) is not available at the BS.

The benefits of IRS in physical layer security under the active attacks have been investigated in the literatures[5–9]. In particular, the performance gains of IRS in terms of security capacity were first explored in a simple model consisting of just one single-antenna LU and one single-antenna ED[5]. Closed-form solutions of the phase shifters of IRS were obtained by leveraging the majorization-minimization (MM) technique[5], with the results indicating better performance than the classical semidefinite relaxation (SDR) method. The authors of Ref. [6] extended the results in Ref. [5] to a multiple-input multiple-output (MIMO) system in which artificial noise (AN) was introduced to enhance security performance. The authors of Ref. [7] further demonstrated that the AN-aided system without an IRS outperforms the IRS-aided system without AN when the IRS is surrounded by a large number of EDs. However, all the above contributions were based on the assumption of a perfect CSI of the eavesdropping channels at the BS. This assumption is too strict and even impractical for two reasons. First, it is quite challenging to estimate the IRS-related channels because the IRS is passive and can neither send nor receive pilot signals. Second, the pilot transmission from the ED to the BS may not be continuous, and the corresponding CSI at the BS may be outdated. In response, robust transmission methods for secure communication of IRS have been proposed to deal with the imperfect CSI of the EDs[8, 9]. In particular, the authors of Ref. [8] proposed a worst-case robust secure transmission strategy under the assumption of an imperfect CSI from the IRS to the ED. Meanwhile, the authors in Ref. [9] considered the more practical, imperfect cascaded BS-IRS-ED channel and proposed an outage-constrained beamforming design method under the statistical CSI error model. However, the authors of that work did not study the imperfect CSI of both LU and ED[9].

To the best of our knowledge, all existing contributions on the IRS-aided security enhancement were developed under the active attack model, in which the BS can acquire the CSI of EDs. At present, no existing work has studied the scenario of passive eavesdropping in IRS-aided secure communication systems. In addition, even for the imperfect CSI under active attacks, the methods proposed in Refs. [8, 9] are only applicable to small-size IRS (i.e., the number of the reflecting elements is less than 10), which can be observed from the numerical results. However, the IRS can be equipped with a large number of reflecting elements for practical IRS-aided communication systems due to the passive feature of the IRS. Furthermore, more reflecting elements can capture greater amounts of electromagnetic energy. In addition, IRS also has advantages over the conventional massive MIMO and relay in terms of energy efficiency, but only when the RIS has a number of reflecting elements[12].

Against the above background, the current paper studies the IRS-aided secrecy communication under the active attacks and passive eavesdropping. The contributions of this paper are summarized as follows:

- This paper proposes an IRS-aided two-phase secrecy communication scheme for a scenario wherein the ED has a similar channel direction as an LU. This scheme is proposed to acquire high-quality eavesdropping information. In specific terms, the BS transmits signals to the LU with low transmission power during the multicasting phase to reduce the information leakage to the ED. In the user cooperation phase, other LUs use the energy harvested in the previous phase to forward the received signals to the attacked LU with the assistance of IRS. Moreover, two models of ED are considered in this work: active attack and passive eavesdropping.
- In the presence of statistical CSI error under the active attack model, we develop an outage-constrained beamforming design, which maximizes the secrecy rate subject to the following constraints: unit-modulus, energy harvesting, and the secrecy rate outage probability constraints. In this case, the outage probability constraint guarantees the maximum secrecy rate of the system to achieve secure communication under a predetermined probability. The nonconvexity of constraints is addressed by resorting to the

Bernstein-Type inequality (BTI) and convex approximations. Then, the active precoders and the passive reflecting beamforming are updated by using the proposed semidefinite programming (SDP) and penalty convex-concave procedure (CCP) technique, respectively, in an iterative manner.

● For the passive ED case with only partial CSI, we maximize an average secrecy rate subject to the unit-modulus constraint of the reflecting beamforming and the energy harvesting constraint. First, an analytically nonconvex angular secrecy model is proposed to address the numerical integration in the objective function. Then a low-complexity algorithm is proposed based on the MM-based alternate optimization (AO) framework. This process involves updating the active beamforming vectors by solving a convex optimization problem. The reflecting beamforming vectors are updated in a closed-form solution that is globally optimal.

● The numerical results demonstrate that the level of the cascaded CSI error plays a vital role in the IRS-aided secure communication systems. Specifically, when the cascaded CSI has a low error, the secrecy rate increases with the number of elements at the IRS due to the increased beamforming gain. However, when the cascaded CSI error is large, the secrecy rate decreases with the number of elements at the IRS due to the increased channel estimation error. Hence, the decision on enabling the IRS to enhance the security capacity in the communication systems depends on the level of the cascaded CSI error. Furthermore, the IRS can enhance the average secrecy rate under passive eavesdropping.

The remainder of this paper is organized as follows: Section 2 introduces the channel model and the system model. Outage constrained robust design problem is formulated for the active eavesdropper model in Section 3. Section 4 further investigates the average eavesdropping rate maximization problem under the passive eavesdropping. Finally, Sections 5 and 6 show the numerical results and conclusions, respectively.

Notations: The following mathematical notations and symbols are used throughout this paper. Vectors and matrices are denoted by boldface lowercase letters and boldface uppercase letters, respectively. The symbols $\boldsymbol{X}^*$, $\boldsymbol{X}^{\mathrm{T}}$, $\boldsymbol{X}^{\mathrm{H}}$, and $\|\boldsymbol{X}\|_F$ denote the conjugate, transpose, Hermitian (conjugate transpose), and Frobenius norm of matrix $\boldsymbol{X}$, respectively. The symbol $\|\boldsymbol{x}\|_2$ denotes 2-norm of vector $\boldsymbol{x}$, while the symbols $\mathrm{Tr}\{\cdot\}$, $\mathrm{Re}(\cdot)$, $|\cdot|$, $\lambda(\cdot)$, and $\angle(\cdot)$ denote the trace, real part, modulus, eigenvalue, and angle of a complex number, respectively. Furthermore, $\mathrm{diag}(\boldsymbol{x})$ is a diagonal matrix with the entries of $\boldsymbol{x}$ on its main diagonal, while $[\boldsymbol{x}]_m$ means the m-th element of the vector $\boldsymbol{x}$. The Kronecker product and the Hadamard product between two matrices, $\boldsymbol{X}$ and $\boldsymbol{Y}$, are denoted by $\boldsymbol{X}\otimes\boldsymbol{Y}$ and $\boldsymbol{X}\odot\boldsymbol{Y}$, respectively. In addition, $\boldsymbol{X}\succcurlyeq\boldsymbol{Y}$ means that $\boldsymbol{X}-\boldsymbol{Y}$ is a positive semidefinite. Finally, the symbol $\mathbb{C}$ denotes complex field, $\mathbb{R}$ represents a real field, $\boldsymbol{I}$ represents the unit matrix, and $\mathrm{j}\triangleq\sqrt{-1}$ is the imaginary unit.

2 System model

As shown in Fig. 1, we consider Rician wiretap channels wherein a BS with N transmit antennas communicates with K single-antenna LUs in the presence of a single-antenna ED. An IRS with M reflecting elements is introduced here to facilitate secure communication.

2.1 Channel model

Let us define the set of all LUs as $\mathcal{K}=\{1,2,...,K\}$, and denote set $\mathcal{K}_{-K}=\mathcal{K}/\{K\}$ and set $\mathcal{K}_{+E}=\mathcal{K}\cup\{E\}$. By denoting $\{D_i,\theta_i\}_{\forall i\in\mathcal{K}_{+E}}$ as the distances and the azimuth angles, from the BS to the LUs and the ED (Fig. 1), respectively, we use the Rician channel to model the corresponding channels $\{\boldsymbol{g}_i\in\mathbb{C}^{N\times 1}\}_{\forall i\in\mathcal{K}_{+E}}$[13]:

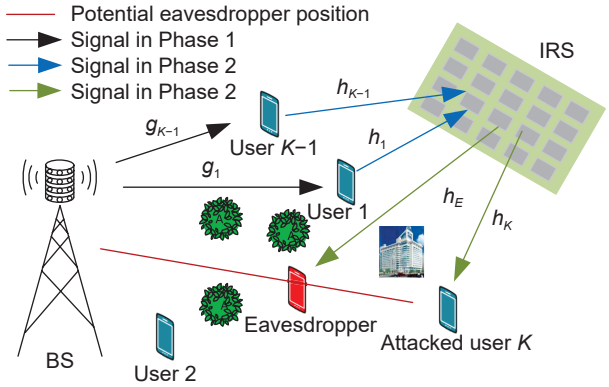

Fig. 1 Two-phase communication system.

$$\boldsymbol{g}_i=\sqrt{\varrho_0\left(\frac{D_i}{d_0}\right)^{-\alpha_{\mathrm{BS}}}}\left(\sqrt{\frac{K_{\mathrm{BS}}}{1+K_{\mathrm{BS}}}}\boldsymbol{g}_i^{\mathrm{LOS}}+\sqrt{\frac{1}{1+K_{\mathrm{BS}}}}\boldsymbol{g}_i^{\mathrm{NLOS}}\right),\forall i\in\mathcal{K}_{+E} \tag{1}$$

where ϱ_0 is the pathloss at the reference distance of d_0, and α_{BS} and K_{BS} are the pathloss exponent and the Rician factor of the BS-related links, respectively. We assume that the BS is equipped with a uniform linear array (ULA). Then, the line-of-sight (LoS) component is given by $\boldsymbol{g}_i^{\mathrm{LOS}}=\left[1,\mathrm{e}^{-\mathrm{j}\pi\sin\theta_i},\ldots,\mathrm{e}^{-\mathrm{j}(N-1)\pi\sin\theta_i}\right]$, and the non-LoS component is drawn from a Rayleigh fading, i.e., $\boldsymbol{g}_i^{\mathrm{NLOS}}\sim\mathcal{CN}(\boldsymbol{0},\boldsymbol{I}_N)$.

Furthermore, by denoting $\{D_{\mathrm{IRS}},\theta_{\mathrm{IRS}}\}$ as the distance and the azimuth angle from the BS to the IRS, we can easily obtain the distances $\{d_{\mathrm{IRS},i}\}_{\forall i\in\mathcal{K}_{+E}}$ and the azimuth angles $\{\varphi_i\}_{\forall i\in\mathcal{K}_{+E}}$ from the IRS to the LUs and the ED as shown in Fig. 2. These are respectively denoted as follows:

$$d_{\mathrm{IRS},i}=\left[(D_{\mathrm{IRS}}\cos\theta_{\mathrm{IRS}}-D_i\cos\theta_i)^2+(D_{\mathrm{IRS}}\sin\theta_{\mathrm{IRS}}-D_i\sin\theta_i)^2\right]^{-1/2},$$

$$\sin\varphi_i=\frac{1}{d_{\mathrm{IRS},i}}(D_i\sin\theta_i-D_{\mathrm{IRS}}\sin\theta_{\mathrm{IRS}}),$$

$$\cos\varphi_i=\frac{1}{d_{\mathrm{IRS},i}}(D_{\mathrm{IRS}}\cos\theta_{\mathrm{IRS}}-D_i\cos\theta_i).$$

The corresponding channels $\{\boldsymbol{h}_i\in\mathbb{C}^{N\times1}\}_{\forall i\in\mathcal{K}_{+E}}$ are given by

$$\boldsymbol{h}_i=\sqrt{\varrho_0\left(\frac{d_{\mathrm{IRS},i}}{d_0}\right)^{-\alpha_{\mathrm{IRS}}}}\left(\sqrt{\frac{K_{\mathrm{IRS}}}{1+K_{\mathrm{IRS}}}}\boldsymbol{h}_i^{\mathrm{LOS}}+\sqrt{\frac{1}{1+K_{\mathrm{IRS}}}}\boldsymbol{h}_i^{\mathrm{NLOS}}\right),\forall i\in\mathcal{K}_{+E} \tag{2}$$

where α_{IRS} and K_{IRS} are the pathloss exponent and the Rician factor of the IRS-related links, respectively, and $\boldsymbol{h}_i^{\mathrm{NLOS}}$ is the non-LoS component, whose distribution is the same as that of $\boldsymbol{g}_i^{\mathrm{NLOS}}$. Assuming an $M=M_x\times M_y$ uniform plane array (UPA) deployed at the IRS with M_x and M_y being the number of reflecting elements in the x-axis and y-axis, respectively, then the LoS component is written as

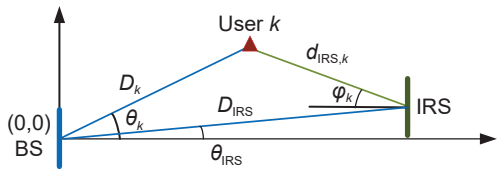

Fig. 2 Coordinates of communication nodes in the system.

$$\boldsymbol{h}_i^{\mathrm{LOS}}=\boldsymbol{h}_i^x\otimes\boldsymbol{h}_i^y \tag{3}$$

where $\boldsymbol{h}_i^x=[1,\ldots,\mathrm{e}^{-\mathrm{j}\pi(M_x-1)\cos\varphi_i\cos\phi\sin\theta_i}]^{\mathrm{T}}$, $\boldsymbol{h}_i^y=[1,\ldots,\mathrm{e}^{-\mathrm{j}\pi(M_x-1)\sin\varphi_i\cos\phi\sin\theta_i}]^{\mathrm{T}}$, and ϕ is the elevation angle observed at the IRS side.

2.2 Signal transmission

We assume that the ED, shown in Fig. 1, hides at the line connecting the BS to one of the users (denoted as user K) to achieve a high attack success rate. In this situation, the signal received by the ED is highly correlated with user K[10, 11], which leads to $\theta_E\approx\theta_K$, $\boldsymbol{g}_E^{\mathrm{LOS}}\approx\boldsymbol{g}_K^{\mathrm{LOS}}$, and $D_E\in(0,D_K)$. The channel $\boldsymbol{g}_E$ is approximately equal to the channel $\boldsymbol{g}_K$ when the Rician factor K_{BS} is sufficiently large.

In particular, in the first phase, the BS multicasts the common signal to all users except user K†. In the second phase, the helping users ($\forall k\in\mathcal{K}_{-K}$) forward the decoded common signal to user K via the IRS. In this work, the LUs adopt the hybrid information and energy harvesting receiving mode to implement the user cooperation scheme without consuming extra energy. This specific mode splits the received signal into two power streams, with power splitting ratios t_k and $1-t_k$: the former is used for decoding the signal and the latter is for harvesting energy.

2.2.1 Multicasting phase

In this phase, the BS multicasts the signal s to the helping LUs through beamforming vector $\boldsymbol{f}\in\mathbb{C}^{N\times1}$ which is limited to the maximum transmit power $P_{\max}$, i.e., $\|\boldsymbol{f}\|_2^2\leqslant P_{\max}$. Given that $\boldsymbol{g}_E\approx\boldsymbol{g}_K$, the beamforming $\boldsymbol{f}$ must satisfy $|\boldsymbol{g}_K^{\mathrm{H}}\boldsymbol{f}|=0$ to ensure that $|\boldsymbol{g}_E^{\mathrm{H}}\boldsymbol{f}|\approx0$. Then, by using the QR decomposition (i.e., $\boldsymbol{Q}^{\mathrm{H}}\boldsymbol{Q}=\boldsymbol{I}$), we let $\boldsymbol{Q}\in\mathbb{C}^{N\times(N-1)}$ be the orthogonal matrix spanning the null space of $\boldsymbol{g}_K$. In this way, we can design $\boldsymbol{f}=\boldsymbol{Q}\boldsymbol{z}$, where $\boldsymbol{z}\in\mathbb{C}^{(N-1)\times1}$ is a newly introduced variable. Therefore, the signal received by LU k is given by $\boldsymbol{g}_k^{\mathrm{H}}\boldsymbol{Q}\boldsymbol{z}+n_k$, where n_k is the received noise with the noise power of σ_k^2. By adopting the hybrid receiving mode and letting $\boldsymbol{t}=[t_1,\ldots,t_{K-1}]^{\mathrm{T}}$, where t_k is the power splitting ratio of LU k, the achievable rate at LU $k\neq K$ can be expressed

† The RIS is assumed to be turned off in the first phase to avoid reflecting useful signals to the ED. Please note that this assumption is practical because the BS has no responsibility of designing secure reflecting beaming for the RIS, which, in turn, reduces the computational complexity and hardware cost at the BS.

as follows:

$$R_k(\boldsymbol{z},t_k)=\frac{1}{2}\log_2\left(1+\frac{t_k}{\sigma_k^2}\left|\boldsymbol{g}_k^{\mathrm{H}}\boldsymbol{Q}\boldsymbol{z}\right|^2\right) \tag{4}$$

where the factor 1/2 is due to the assumption that the total time duration is evenly distributed to two transmission phases. The harvested power at LU $k\neq K$ is given by

$$(1-t_k)\left|\boldsymbol{g}_k^{\mathrm{H}}\boldsymbol{Q}\boldsymbol{z}\right|^2 \tag{5}$$

2.2.2 User cooperation phase

In this phase, the helping LUs ($\forall k\in\mathcal{K}_{-K}$) use the power harvested in the multicasting phase to forward the signal s to LU K through a beamforming vector $\boldsymbol{w}\in\mathbb{C}^{(K-1)\times 1}=[w_1,...,w_{K-1}]^{\mathrm{T}}$. Here, the direct links between the helping LUs and the LU K may be blocked, given that LU K is randomly selected by the ED and assuming that there are many obstacles in the communication environment (e.g., indoor applications). To address this issue, an IRS can be installed on a building with a certain height. Thus, the IRS is capable of reflecting the signals forwarded by the helping LUs to LU K. We denote $\boldsymbol{e}$ as the reflection coefficient vector of the IRS, where $|e_m|^2=1$, $\forall m=1,\ldots,M$. On one hand, the signal received by LU K is given by

$$y_K=\boldsymbol{h}_K^{\mathrm{H}}\mathrm{diag}(\boldsymbol{e}^*)\boldsymbol{H}_{\mathrm{IRS}}\boldsymbol{w}s+n_K=\boldsymbol{e}^{\mathrm{H}}\boldsymbol{H}_K\boldsymbol{w}s+n_K,$$

where $\boldsymbol{H}_{\mathrm{IRS}}=[\boldsymbol{h}_1,...,\boldsymbol{h}_{K-1}]$, $\boldsymbol{H}_K=\left[\boldsymbol{h}_K^*\odot\boldsymbol{h}_1,...,\boldsymbol{h}_K^*\odot\boldsymbol{h}_{K-1}\right]$ is the cascaded LU-IRS-LU (LIL) channel, and $n_K\sim\mathcal{CN}(\boldsymbol{0},\sigma_K^2)$ is the noise. The corresponding achievable rate is expressed as

$$R_K(\boldsymbol{w},\boldsymbol{e})=\frac{1}{2}\log_2\left(1+\frac{1}{\sigma_K^2}\left|\boldsymbol{e}^{\mathrm{H}}\boldsymbol{H}_K\boldsymbol{w}\right|^2\right) \tag{6}$$

On the other hand, the signal received by the ED is expressed as $y_E=\boldsymbol{e}^{\mathrm{H}}\boldsymbol{H}_E\boldsymbol{w}s+n_E$, where $\boldsymbol{H}_E=\left[\boldsymbol{h}_E^*\odot\boldsymbol{h}_1,...,\boldsymbol{h}_E^*\odot\boldsymbol{h}_{K-1}\right]$ is the cascaded LU-IRS-ED (LIE) channel, and $n_E\sim\mathcal{CN}(\boldsymbol{0},\sigma_E^2)$ is the received noise at the ED.

The corresponding eavesdropping rate is given by

$$R_E(\boldsymbol{w},\boldsymbol{e})=\frac{1}{2}\log_2\left(1+\frac{1}{\sigma_E^2}\left|\boldsymbol{e}^{\mathrm{H}}\boldsymbol{H}_E\boldsymbol{w}\right|^2\right) \tag{7}$$

Finally, the secrecy rate of this system under the user cooperation scheme can be expressed as follows[11]:

$$\left[\min_{\forall k\in\mathcal{K}}R_k-R_E\right]^+ \tag{8}$$

In the following two sections, we consider the system design for two ED models: the active ED model and the passive ED model.

3 ED model I: Active ED model

In this section, we consider the active attack case, in which the ED pretends to be an LU sending pilot signals to the transmitters (including the BS and the helping LUs), during the channel estimation procedure[10, 11]. It is reasonable to assume that the BS can obtain the perfect system CSI by capably addressing this attack by using the multi-antenna technique. Nevertheless, the single-antenna helping LUs only have the imperfect CSI of LU K and the ED due to their limited anti-interference ability.

3.1 Channel uncertainties

Based on the above assumption, the cascaded channels can be modeled as follows:

$$\boldsymbol{H}_K=\widehat{\boldsymbol{H}}_K+\Delta_K,\boldsymbol{H}_E=\widehat{\boldsymbol{H}}_E+\Delta_E \tag{9}$$

where $\widehat{\boldsymbol{H}}_K$ and $\widehat{\boldsymbol{H}}_E$ are the estimated cascaded channels, $\Delta_K=[\Delta_1^K,...,\Delta_{K-1}^K]$ and $\Delta_E=[\Delta_1^E,...,\Delta_{K-1}^E]$ are the unknown cascaded channel errors, and Δ_k^K and Δ_k^E are the unknown cascaded LIL and LIE channel error vectors at LU k, respectively.

According to Ref. [14], the robust beamforming under the statistical CSI error model outperforms the bounded CSI error model in terms of convergence speed, minimum transmit power, and computational complexity. Furthermore, the statistical channel error model is more suitable in modeling the channel estimation error when the channel estimation is based on the minimum mean sum error (MMSE) method. Hence, we adopt the statistical model to characterize the cascaded CSI imperfection[14]. In other words, each CSI error vector is assumed to follow the circularly symmetric complex Gaussian (CSCG) distribution, i.e.,

$$\Delta_k^K\sim\mathcal{CN}(\boldsymbol{0},\boldsymbol{\Sigma}_k^K),\boldsymbol{\Sigma}_k^K\succcurlyeq\boldsymbol{0},\forall k\in\mathcal{K}_{-K} \tag{10a}$$

$$\Delta_k^E\sim\mathcal{CN}(\boldsymbol{0},\boldsymbol{\Sigma}_k^E),\boldsymbol{\Sigma}_k^E\succcurlyeq\boldsymbol{0},\forall k\in\mathcal{K}_{-K} \tag{10b}$$

where $\boldsymbol{\Sigma}_k^K\in\mathbb{C}^{M\times M}$ and $\boldsymbol{\Sigma}_k^E\in\mathbb{C}^{M\times M}$ are positive semidefinite error covariance matrices. Note that the

CSI error vectors of different LUs are independent of one another. Therefore, we have

$$\mathrm{vec}(\Delta_K) \sim \mathcal{CN}(\mathbf{0}, \mathbf{\Sigma}_K), \mathrm{vec}(\Delta_E) \sim \mathcal{CN}(\mathbf{0}, \mathbf{\Sigma}_E) \tag{11}$$

where $\mathbf{\Sigma}_K$ and $\mathbf{\Sigma}_E$ are block diagonal matrices, i.e., $\mathbf{\Sigma}_K = \mathrm{diag}(\mathbf{\Sigma}_1^K, ..., \mathbf{\Sigma}_{K-1}^K)$ and $\mathbf{\Sigma}_E = \mathrm{diag}(\mathbf{\Sigma}_1^E, ..., \mathbf{\Sigma}_{K-1}^E)$.

3.2 Outage-constrained beamforming design

Following the statistical CSI error model, we develop a robust probabilistic algorithm for the secrecy rate maximization problem. This is formulated as

$$\max_{R_{\mathrm{sec}}, \boldsymbol{z}, \boldsymbol{w}, \boldsymbol{e}, \boldsymbol{t}} R_{\mathrm{sec}} \tag{12a}$$

$$\text{s.t. } \Pr\left\{\min_{\forall k \in \mathcal{K}} R_k - R_E \geqslant R_{\mathrm{sec}}\right\} \geqslant 1-\rho \tag{12b}$$

$$\|\boldsymbol{z}\|_2^2 \leqslant P_{\max} \tag{12c}$$

$$|e_m|^2 = 1, 1 \leqslant m \leqslant M \tag{12d}$$

$$0 \leqslant t \leqslant 1 \tag{12e}$$

$$|w_k|^2 \leqslant (1-t_k)\left|\boldsymbol{g}_k^{\mathrm{H}} \boldsymbol{Q} \boldsymbol{z}\right|^2, \forall k \in \mathcal{K}_{-K} \tag{12f}$$

where $\rho \in (0, 1]$ is the secrecy rate outage probability.

Problem (12) is difficult to solve due to the computationally intractable rate outage probability constraint (12b), the nonconvex unit-modulus constraint (12d), and the nonconvex power constraint (12f).

First, we replace constraint (12b) with the development of a safe approximation, consisting of three steps, as explained below.

Step 1 Decouple the probabilistic constraint: First of all, based on the independence between $\{\boldsymbol{g}_k\}_{\forall k \in \mathcal{K}_{-K}}$ and $\boldsymbol{H}_K$, we have

$$\text{Formula (12b)} \Leftrightarrow \prod_{k=1}^{K} \Pr\{R_k - R_E \geqslant R_{\mathrm{sec}}\} \geqslant 1-\rho \tag{13}$$

$$\Leftarrow \Pr\{R_k - R_E \geqslant R_{\mathrm{sec}}\} \geqslant 1-\bar{\rho}, \forall k \in \mathcal{K}_K \tag{14}$$

where $\bar{\rho} = 1-(1-\rho)^{1/K}$.

Step 2 Convenient approximations: To address the nonconcavity of $R_k - R_E, \forall k \in \mathcal{K}_K$, we must construct a sequence of surrogate functions of $\{R_i\}_{\forall i \in \mathcal{K}_{+E}}$. Specifically, we need the following lemmas.

Lemma 1[15] The quadratic-over-linear function $\frac{x^2}{y}$ is jointly convex in (x, y) and lower bounded by its linear first-order Taylor approximation $\frac{2x^{(n)}}{y^{(n)}}x - (\frac{x^{(n)}}{y^{(n)}})^2 y$ at a fixed point $(x^{(n)}, y^{(n)})$.

We substitute x with $\boldsymbol{g}_k^{\mathrm{H}}\boldsymbol{Q}\boldsymbol{z}$ and y with $1/t_k$ to utilize Lemma 1 and obtain a concave lower bound of rate $R_k(\boldsymbol{z}, t_k)$ for $\forall k \in \mathcal{K}_{-K}$. The lower bound is given by

$$\begin{aligned}\widetilde{R}_k(\boldsymbol{z}, t_k | \boldsymbol{z}^{(n)}, t_k^{(n)}) = \frac{1}{2}\log_2\Bigg(1 - \frac{t_k^{(n),2}}{\sigma_k^2 t_k}\left|\boldsymbol{g}_k^{\mathrm{H}}\boldsymbol{Q}\boldsymbol{z}^{(n)}\right|^2 + \\ 2t_k^{(n)}\mathrm{Re}\left(\frac{1}{\sigma_k^2}\boldsymbol{z}^{(n),\mathrm{H}}\boldsymbol{Q}^{\mathrm{H}}\boldsymbol{g}_k\boldsymbol{g}_k^{\mathrm{H}}\boldsymbol{Q}\boldsymbol{z}\right)\Bigg)\end{aligned} \tag{15}$$

for any feasible solution $\{\boldsymbol{z}^{(n)}, t_k^{(n)}\}$.

Lemma 2 The upper bound of rate $R_E(\boldsymbol{w}, \boldsymbol{e})$ is given by

$$\widetilde{R}_E(\boldsymbol{w}, \boldsymbol{e}, a_E) = \frac{a_E\left|\boldsymbol{e}^{\mathrm{H}}\boldsymbol{H}_E\boldsymbol{w}\right|^2/\sigma_E^2 + a_E - \ln a_E - 1}{2\ln 2},$$

where a_E serves as the auxiliary variable.

Proof: See Appendix A.

Lemma 3 The lower bound of rate $R_K(\boldsymbol{w}, \boldsymbol{e})$ is given by

$$\begin{aligned}\widetilde{R}_K(\boldsymbol{w}, \boldsymbol{e}, a_K, v) = \frac{1}{2\ln 2}\Big(-a_K|v|^2|\boldsymbol{e}^{\mathrm{H}}\boldsymbol{H}_K\boldsymbol{w}|^2 + 1 - \\ \sigma_K^2 a_K|v|^2 + 2a_K\mathrm{Re}\left(v\boldsymbol{e}^{\mathrm{H}}\boldsymbol{H}_K\boldsymbol{w}\right) - a_K + \ln a_K\Big),\end{aligned}$$

where a_K and v are the auxiliary variables.

Proof: See Appendix B.

For the convenience of derivations, we assume that $\mathbf{\Sigma}_k^K = \varepsilon_{K,k}^2\boldsymbol{I}_M$ and $\mathbf{\Sigma}_k^E = \varepsilon_{E,k}^2\boldsymbol{I}_M$, then $\mathbf{\Sigma}_K = \mathbf{\Lambda}_K \otimes \boldsymbol{I}_M$ where $\mathbf{\Lambda}_K = \mathrm{diag}(\varepsilon_{K,1}^2, ..., \varepsilon_{K,K-1}^2)$, and $\mathbf{\Sigma}_E = \mathbf{\Lambda}_E \otimes \boldsymbol{I}_M$ where $\mathbf{\Lambda}_E = \mathrm{diag}(\varepsilon_{E,1}^2, ..., \varepsilon_{E,K-1}^2)$. Furthermore, the error vectors in Formula (11) can be reconfigured as follows: $\mathrm{vec}(\Delta_K) = \mathbf{\Sigma}_K^{\frac{1}{2}}\boldsymbol{i}_K$ where $\boldsymbol{i}_K \sim \mathcal{CN}(\mathbf{0}, \boldsymbol{I}_{M(K-1)})$, and $\mathrm{vec}(\Delta_E) = \mathbf{\Sigma}_E^{\frac{1}{2}}\boldsymbol{i}_E$ where $\boldsymbol{i}_E \sim \mathcal{CN}(\mathbf{0}, \boldsymbol{I}_{M(K-1)})$. Then, we define $\boldsymbol{E} = \boldsymbol{e}\boldsymbol{e}^{\mathrm{H}}$ and $\boldsymbol{W} = \boldsymbol{w}\boldsymbol{w}^{\mathrm{H}}$. Upon combining Eq. (15) with Lemma 2, the left-hand side (LHS) of Formula (14) corresponding to the users in $\mathcal{K}_{-K}$ can be replaced by its lower bound:

$$\begin{aligned}&\Pr\{R_k - R_E \geqslant R_{\mathrm{sec}}\} \geqslant \\ &\Pr\left\{\widetilde{R}_k - \widetilde{R}_E \geqslant R_{\mathrm{sec}}\right\} = \\ &\Pr\Big\{a_E\mathrm{Tr}\left(\boldsymbol{E}(\widehat{\boldsymbol{H}}_E + \Delta_E)\boldsymbol{W}(\widehat{\boldsymbol{H}}_E^{\mathrm{H}} + \Delta_E^{\mathrm{H}})\right) - \\ &[2\ln 2(\widetilde{R}_k - R_{\mathrm{sec}}) - a_E + \ln a_E + 1]\sigma_E^2 \leqslant 0\Big\} = \\ &\Pr\left\{\boldsymbol{i}_E^{\mathrm{H}}\boldsymbol{U}_E\boldsymbol{i}_E + 2\mathrm{Re}\left(\boldsymbol{u}_E^{\mathrm{H}}\boldsymbol{i}_E\right) + u_k \leqslant 0\right\}\end{aligned} \tag{16}$$

where

$$\boldsymbol{U}_E = a_E\mathbf{\Sigma}_E^{\frac{1}{2}}(\boldsymbol{W}^{\mathrm{T}} \otimes \boldsymbol{E})\mathbf{\Sigma}_E^{\frac{1}{2}} \tag{17a}$$

$$\boldsymbol{u}_E = a_E \boldsymbol{\Sigma}_E^{\frac{1}{2}} \mathrm{vec}(\boldsymbol{E}\widehat{\boldsymbol{H}}_E \boldsymbol{W}) \tag{17b}$$

$$\begin{aligned} u_k =& a_E \mathrm{Tr}\left(\boldsymbol{E}\widehat{\boldsymbol{H}}_E \boldsymbol{W} \widehat{\boldsymbol{H}}_E^{\mathrm{H}}\right) - [(\widetilde{R}_k - R_{\mathrm{sec}}) 2\ln 2 - \\ & a_E + \ln a_E + 1]\sigma_E^2 \end{aligned} \tag{17c}$$

Combining Lemma 2 with Lemma 3, the LHS of Formula (14) corresponding to LU K can be replaced by its lower bound:

$$\begin{aligned} &\Pr\{R_K - R_E \geqslant R_{\mathrm{sec}}\} \geqslant \\ &\Pr\left\{\widetilde{R}_K - \widetilde{R}_E \geqslant R_{\mathrm{sec}}\right\} = \\ &\Pr\Big\{a_K |v|^2 \mathrm{Tr}\left(\boldsymbol{E}(\widehat{\boldsymbol{H}}_K + \Delta_K)\boldsymbol{W}(\widehat{\boldsymbol{H}}_K^{\mathrm{H}} + \Delta_K^{\mathrm{H}})\right) - \\ &2a_K \mathrm{Re}\left\{v\boldsymbol{e}^{\mathrm{H}}(\widehat{\boldsymbol{H}}_K + \Delta_K)\boldsymbol{w}\right\} - c + \\ &\frac{a_E}{\sigma_E^2}\mathrm{Tr}\left(\boldsymbol{E}(\widehat{\boldsymbol{H}}_E + \Delta_E)\boldsymbol{W}(\widehat{\boldsymbol{H}}_E^{\mathrm{H}} + \Delta_E^{\mathrm{H}})\right) \leqslant 0\Big\} = \\ &\Pr\left\{\boldsymbol{i}^{\mathrm{H}}\boldsymbol{U}_K\boldsymbol{i} + 2\mathrm{Re}\left\{\boldsymbol{u}_K^{\mathrm{H}}\boldsymbol{i}\right\} + u_K \leqslant 0\right\} \end{aligned} \tag{18}$$

where

$$\boldsymbol{i} = [\ \boldsymbol{i}_K^{\mathrm{H}},\quad \boldsymbol{i}_E^{\mathrm{H}}\ ]^{\mathrm{H}} \tag{19a}$$

$$\begin{aligned} \boldsymbol{U}_K = \mathrm{diag}\Big\{ & a_K |v|^2 \boldsymbol{\Sigma}_K^{\frac{1}{2}}(\boldsymbol{W}^{\mathrm{T}} \otimes \boldsymbol{E})\boldsymbol{\Sigma}_K^{\frac{1}{2}}, \\ & \frac{a_E}{\sigma_E^2}\boldsymbol{\Sigma}_E^{\frac{1}{2}}(\boldsymbol{W}^{\mathrm{T}} \otimes \boldsymbol{E})\boldsymbol{\Sigma}_E^{\frac{1}{2}}\Big\} \end{aligned} \tag{19b}$$

$$\begin{aligned} \boldsymbol{u}_K = \Big[& a_K |v|^2 \mathrm{vec}^{\mathrm{H}}(\boldsymbol{E}\widehat{\boldsymbol{H}}_K \boldsymbol{W})\boldsymbol{\Sigma}_K^{\frac{1}{2}} - a_K v \mathrm{vec}^{\mathrm{H}}(\boldsymbol{e}\boldsymbol{w}^{\mathrm{H}})\boldsymbol{\Sigma}_K^{\frac{1}{2}}, \\ & \frac{a_E}{\sigma_E^2}\mathrm{vec}^{\mathrm{H}}(\boldsymbol{E}\widehat{\boldsymbol{H}}_E \boldsymbol{W})\boldsymbol{\Sigma}_E^{\frac{1}{2}}\Big]^{\mathrm{H}} \end{aligned} \tag{19c}$$

$$\begin{aligned} u_K = & a_K |v|^2 \mathrm{Tr}\left(\boldsymbol{E}\widehat{\boldsymbol{H}}_K \boldsymbol{W} \widehat{\boldsymbol{H}}_K^{\mathrm{H}}\right) + \frac{a_E}{\sigma_E^2}\mathrm{Tr}\left(\boldsymbol{E}\widehat{\boldsymbol{H}}_E \boldsymbol{W} \widehat{\boldsymbol{H}}_E^{\mathrm{H}}\right) - \\ & 2a_K \mathrm{Re}\left(v\boldsymbol{e}^{\mathrm{H}}\widehat{\boldsymbol{H}}_K \boldsymbol{w}\right) - c \end{aligned} \tag{19d}$$

$$\begin{aligned} c = & \ln a_E + \ln a_K - a_E - a_K - 2R_{\mathrm{sec}} \ln 2 - \\ & \sigma_K^2 a_K |v|^2 + 2 \end{aligned} \tag{19e}$$

Now, by substituting Formulas (16) and (18) into Formula (14), then Formula (14) can be approximated as follows:

$$\Pr\left\{\boldsymbol{i}_E^{\mathrm{H}}\boldsymbol{U}_E\boldsymbol{i}_E + 2\mathrm{Re}\left(\boldsymbol{u}_E^{\mathrm{H}}\boldsymbol{i}_E\right) + u_k \leqslant 0\right\} \geqslant 1 - \bar{\rho}, \quad \forall k \in \mathcal{K}_{-K} \tag{20a}$$

$$\Pr\left\{\boldsymbol{i}^{\mathrm{H}}\boldsymbol{U}_K\boldsymbol{i} + 2\mathrm{Re}\left(\boldsymbol{u}_K^{\mathrm{H}}\boldsymbol{i}\right) + u_K \leqslant 0\right\} \geqslant 1 - \bar{\rho} \tag{20b}$$

Step 3 A BTI-based Safe Approximation: The outage probabilities in Formula (20) are characterized by quadratic inequalities, which can be safely approximated by using the following lemma.

Lemma 4 (BTI)[16] Let us assume that $f(\boldsymbol{x}) = \boldsymbol{x}^{\mathrm{H}}\boldsymbol{U}\boldsymbol{x} + 2\mathrm{Re}(\boldsymbol{u}^{\mathrm{H}}\boldsymbol{x}) + u$, where $\boldsymbol{U} \in \mathbb{C}^{n\times n}$, $\boldsymbol{u} \in \mathbb{C}^{n\times 1}$, $u \in \mathbb{R}$, and $\boldsymbol{x} \in \mathbb{C}^{n\times 1} \sim \mathcal{CN}(\boldsymbol{0}, \boldsymbol{I})$. Then for any $\rho \in [0,1]$, the following approximation holds:

$$\begin{aligned} & \Pr\{\boldsymbol{x}^{\mathrm{H}}\boldsymbol{U}\boldsymbol{x} + 2\mathrm{Re}(\boldsymbol{u}^{\mathrm{H}}\boldsymbol{x}) + u \leqslant 0\} \geqslant 1 - \rho \\ \Rightarrow & \mathrm{Tr}\{\boldsymbol{U}\} + \sqrt{2\ln(1/\rho)}x - \ln(\rho)\lambda_{\max}^{+}(\boldsymbol{U}) + u \leqslant 0 \\ \Rightarrow & \begin{cases} \mathrm{Tr}\{\boldsymbol{U}\} + \sqrt{2\ln(1/\rho)}x - \ln(\rho)y + u \leqslant 0, \\ \sqrt{\|\boldsymbol{U}\|_F^2 + 2\|\boldsymbol{u}\|_2^2} \leqslant x, \\ y\boldsymbol{I} - \boldsymbol{U} \succcurlyeq \boldsymbol{0}, y \geqslant 0 \end{cases} \end{aligned} \tag{21}$$

where $\lambda_{\max}^{+}(\boldsymbol{U}) = \max(\lambda_{\max}(\boldsymbol{U}), 0)$. x and y are slack variables.

Before using Lemma 4, we need the following simplified derivations for LU k, $\forall k \in \mathcal{K}_{-K}$:

$$\begin{aligned} \mathrm{Tr}\{\boldsymbol{U}_E\} = & \mathrm{Tr}\left\{a_E \boldsymbol{\Sigma}_E^{\frac{1}{2}}(\boldsymbol{W}^{\mathrm{T}} \otimes \boldsymbol{E})\boldsymbol{\Sigma}_E^{\frac{1}{2}}\right\} = \\ & \mathrm{Tr}\left\{a_E(\boldsymbol{W}^{\mathrm{T}} \otimes \boldsymbol{E})(\boldsymbol{\Lambda}_E \otimes \boldsymbol{I}_M)\right\} = \\ & a_E M \mathrm{Tr}\{\boldsymbol{\Lambda}_E \boldsymbol{W}\} \end{aligned} \tag{22a}$$

$$\|\boldsymbol{U}_E\|_F^2 = a_E^2 M^2 \|\boldsymbol{\Lambda}_E \boldsymbol{W}\|_F^2 \tag{22b}$$

$$\begin{aligned} \|\boldsymbol{u}_E\|_2^2 = & a_E^2 \mathrm{vec}^{\mathrm{H}}(\boldsymbol{E}\widehat{\boldsymbol{H}}_E \boldsymbol{W})(\boldsymbol{\Lambda}_E \otimes \boldsymbol{I}_M)\mathrm{vec}(\boldsymbol{E}\widehat{\boldsymbol{H}}_E \boldsymbol{W}) = \\ & a_E^2 M \|\boldsymbol{\Lambda}_E^{\frac{1}{2}} \boldsymbol{W} \widehat{\boldsymbol{H}}_E^{\mathrm{H}} \boldsymbol{e}\|_2^2 \end{aligned} \tag{22c}$$

$$\begin{aligned} \lambda_{\max}(\boldsymbol{U}_E) = & \lambda_{\max}(a_E \boldsymbol{\Sigma}_E^{\frac{1}{2}}(\boldsymbol{W}^{\mathrm{T}} \otimes \boldsymbol{E})\boldsymbol{\Sigma}_E^{\frac{1}{2}}) = \\ & \lambda_{\max}(a_E(\boldsymbol{\Lambda}_E \boldsymbol{W}^{\mathrm{T}} \otimes \boldsymbol{E})) = \\ & a_E \lambda_{\max}(\boldsymbol{\Lambda}_E \boldsymbol{W})\lambda(\boldsymbol{E}) = \\ & a_E M \boldsymbol{w}^{\mathrm{H}} \boldsymbol{\Lambda}_E \boldsymbol{w} \end{aligned} \tag{22d}$$

By substituting Eq. (22) into Formula (21) and introducing slack variables $\{x_E, y_E\}$, the constraints for $\forall k \in \mathcal{K}_{-K}$ in Formula (20a) are transformed into the following deterministic form:

$$\mathrm{BTI}_1 \triangleq \begin{cases} \mathrm{Tr}\{\boldsymbol{U}_E\} + \sqrt{2\ln(1/\bar{\rho})}x_E - \ln(\bar{\rho})y_E + \\ \quad u_k \leqslant 0, \forall k \in \mathcal{K}_{-K}; \\ \left\| \begin{matrix} a_E M \mathrm{vec}(\boldsymbol{\Lambda}_E \boldsymbol{W}) \\ \sqrt{2M} a_E \boldsymbol{\Lambda}_E^{\frac{1}{2}} \boldsymbol{W} \widehat{\boldsymbol{H}}_E^{\mathrm{H}} \boldsymbol{e} \end{matrix} \right\| \leqslant x_E, \\ \quad y_E \geqslant a_E M \boldsymbol{w}^{\mathrm{H}} \boldsymbol{\Lambda}_E \boldsymbol{w} \end{cases} \tag{23}$$

Meanwhile, the simplified derivations for LU K are given as follows:

$$\mathrm{Tr}\{\boldsymbol{U}_K\} = a_K |v|^2 M \mathrm{Tr}\{\boldsymbol{\Lambda}_K \boldsymbol{W}\} + \frac{a_E}{\sigma_E^2} M \mathrm{Tr}\{\boldsymbol{\Lambda}_E \boldsymbol{W}\} \tag{24a}$$

$$\|\boldsymbol{U}_K\|_F^2 = a_K^2 |v|^4 M^2 \|\boldsymbol{\Lambda}_K \boldsymbol{W}\|_F^2 + \frac{a_E^2}{\sigma_E^4} M^2 \|\boldsymbol{\Lambda}_E \boldsymbol{W}\|_F^2 \tag{24b}$$

$$\|\boldsymbol{u}_K\|^2 = M\|\boldsymbol{\Lambda}_K^{\frac{1}{2}}\left(a_K|v|^2\boldsymbol{W}\widehat{\boldsymbol{H}}_K^{\mathrm{H}}\boldsymbol{e} - a_K v\boldsymbol{w}\right)\|_2^2 + \frac{a_E^2}{\sigma_E^4}M\|\boldsymbol{e}^{\mathrm{H}}\widehat{\boldsymbol{H}}_E\boldsymbol{W}\boldsymbol{\Lambda}_E^{\frac{1}{2}}\|_2^2 \tag{24c}$$

$$\lambda_{\max}(\boldsymbol{U}_K) = \max\{a_K|v|^2M\boldsymbol{w}^{\mathrm{H}}\boldsymbol{\Lambda}_K\boldsymbol{w}, \frac{a_E}{\sigma_E^2}M\boldsymbol{w}^{\mathrm{H}}\boldsymbol{\Lambda}_E\boldsymbol{w}\} \tag{24d}$$

By substituting the above equations into Formula (21) and introducing slack variables $\{x_K, y_K\}$, the constraint for LU K in Formula (20b) is transformed into the following deterministic form:

$$\mathrm{BTI}_2 \triangleq \begin{cases} \mathrm{Tr}\{\boldsymbol{U}_K\} + \sqrt{2\ln(1/\bar{\rho})}x_K - \ln(\bar{\rho})y_K + u_K \leqslant 0, \\ \left\| \begin{array}{c} a_K|v|^2M\mathrm{vec}(\boldsymbol{\Lambda}_K\boldsymbol{W}) \\ a_EM\mathrm{vec}(\boldsymbol{\Lambda}_E\boldsymbol{W})/\sigma_E^2 \\ \sqrt{2M}\boldsymbol{\Lambda}_K^{\frac{1}{2}}\left(a_K|v|^2\boldsymbol{W}\widehat{\boldsymbol{H}}_K^{\mathrm{H}}\boldsymbol{e} - a_K v\boldsymbol{w}\right) \\ \sqrt{2M}a_E\boldsymbol{\Lambda}_E^{\frac{1}{2}}\boldsymbol{W}\widehat{\boldsymbol{H}}_E^{\mathrm{H}}\boldsymbol{e}/\sigma_E^2 \end{array} \right\| \leqslant x_K, \\ y_K \geqslant \lambda_{\max}(\boldsymbol{U}_K), y_K \geqslant 0 \end{cases} \tag{25}$$

Then, in order to handle the nonconvex power constraint (12f), we replace the right-hand side (RHS) of Formula (12f) with its linear lower bound:

$$\Xi(z, t_k) = 2(1-t_k^{(n)})\mathrm{Re}\left(z^{(n),\mathrm{H}}\boldsymbol{Q}^{\mathrm{H}}\boldsymbol{g}_k\boldsymbol{g}_k^{\mathrm{H}}\boldsymbol{Q}z\right) - \frac{(1-t_k^{(n)})^2\left|\boldsymbol{g}_k^{\mathrm{H}}\boldsymbol{Q}z^{(n)}\right|^2}{(1-t_k)} \tag{26}$$

at feasible point $\{z^{(n)}, t_k^{(n)}\}$ by adopting the same first-order Taylor approximation used in Lemma 1.

Therefore, based on Foumulas (23) and (25) and Eq. (26) and defining $\boldsymbol{x} = [x_E, x_K]^{\mathrm{T}}$ and $\boldsymbol{y} = [y_E, y_K]^{\mathrm{T}}$, Problem (12) can be approximated as

$$\max_{R_{\mathrm{sec}}, \boldsymbol{z}, \boldsymbol{w}, \boldsymbol{e}, \boldsymbol{t}, a_K, a_E, v, \boldsymbol{x}, \boldsymbol{y}} R_{\mathrm{sec}} \tag{27a}$$

$$\text{s.t. Foumulas (12c)} - \text{(12e)}, (23), (25) \tag{27b}$$

$$|w_k|^2 \leqslant \Xi(\mathbf{z}, t_k), \forall k \in \mathcal{K}_{-K} \tag{27c}$$

Next, we introduce a new variable $\boldsymbol{W} = \boldsymbol{w}\boldsymbol{w}^{\mathrm{H}}$ with $\mathrm{rank}(\boldsymbol{W}) = 1$ for a given $\{\boldsymbol{e}, a_K, a_E, v\}$. However, different from the general SDP, $\boldsymbol{w}$ and $\boldsymbol{W}$ coexist in Eq. (24c). Therefore, the SDR technique is not applicable in this case. To handle this problem, we assume that $\boldsymbol{w}$ and $\boldsymbol{W}$ are two different variables. If $\mathrm{Tr}\{\boldsymbol{W}\} = \lambda_{\max}(\boldsymbol{W})$, then we have $\mathrm{rank}(\boldsymbol{W}) = 1$. If the obtained $\boldsymbol{W}$ is not rank one, we will have $\mathrm{Tr}\{\boldsymbol{W}\} - \lambda_{\max}(\boldsymbol{W}) > 0$. Therefore, we constrain $\mathrm{Tr}\{\boldsymbol{W}\} - \lambda_{\max}(\boldsymbol{W})$ to be less than a very small real positive number threshold ε so as to guarantee the rank-1 condition of $\boldsymbol{W}$, thus yielding the surrogate constraint of rank-1 constraint as

$$\mathrm{Tr}\{\boldsymbol{W}\} - \lambda_{\max}(\boldsymbol{W}) \leqslant \varepsilon \tag{28}$$

When $\mathrm{rank}(\boldsymbol{W}) \approx 1$, the relationship between $\boldsymbol{w}$ and $\boldsymbol{W}$ is given by the following constraint:

$$-\varepsilon \leqslant \|\boldsymbol{w}\|^2 - \mathrm{Tr}\{\boldsymbol{W}\} \leqslant \varepsilon \tag{29}$$

As for constraint (28), as $\lambda_{\max}(\boldsymbol{W})$ is a convex function of $\boldsymbol{W}$[15], the LHS of Formula (28) is concave, which is the difference between a linear function and a convex function. Hence, we need to construct a convex approximation of constraint (28). To address this issue, we introduce the following lemma.

Lemma 5 Denote $\boldsymbol{v}_{max}$ as the eigenvector corresponding to the maximum eigenvalue of a matrix $\boldsymbol{V}$. Thus, we have

$$\mathrm{Tr}\{\boldsymbol{v}_{max}\boldsymbol{v}_{max}^{\mathrm{H}}(\boldsymbol{Z}-\boldsymbol{V})\} = \boldsymbol{v}_{max}^{\mathrm{H}}\boldsymbol{Z}\boldsymbol{v}_{max} - \boldsymbol{v}_{max}^{\mathrm{H}}\boldsymbol{V}\boldsymbol{v}_{max} = \boldsymbol{v}_{max}^{\mathrm{H}}\boldsymbol{Z}\boldsymbol{v}_{max} - \lambda_{\max}(\boldsymbol{V}) \leqslant \lambda_{\max}(\boldsymbol{Z}) - \lambda_{\max}(\boldsymbol{V})$$

for any Hermitian matrix $\boldsymbol{Z}$.

Let $\boldsymbol{d}_{\mathbf{W}}^{(n)}$ be the eigenvector corresponding to the maximum eigenvalue of the feasible point $\boldsymbol{W}^{(n)}$. Then, by using Lemma 5, the surrogate convex constraint of Formula (28) is given by

$$\mathrm{Tr}\{\boldsymbol{W}\} - \lambda_{\max}(\boldsymbol{W}^{(n)}) - \mathrm{Tr}\left\{\boldsymbol{d}_{\boldsymbol{W}}^{(n)}\boldsymbol{d}_{\boldsymbol{W}}^{(n),\mathrm{H}}(\boldsymbol{W}-\boldsymbol{W}^{(n)})\right\} \leqslant \varepsilon \tag{30}$$

Now, we consider constraint (29). By applying the first-order Taylor approximation to $\|\boldsymbol{w}\|^2$, we obtain the following convex approximation of the constraint in Formula (29) as follows:

$$\|\boldsymbol{w}\|^2 - \mathrm{Tr}\{\boldsymbol{W}\} \leqslant \varepsilon \tag{31a}$$

$$2\mathrm{Re}\left(\boldsymbol{w}^{(n),\mathrm{H}}\boldsymbol{w}\right) - \|\boldsymbol{w}^{(n)}\|^2 - \mathrm{Tr}\{\boldsymbol{W}\} \geqslant -\varepsilon \tag{31b}$$

Finally, the subproblem w.r.t., $\{\boldsymbol{z}, \boldsymbol{w}, \boldsymbol{W}, \boldsymbol{t}\}$ is formulated as

$$\max_{R_{\mathrm{sec}}, \boldsymbol{z}, \boldsymbol{w}, \boldsymbol{W}, \boldsymbol{t}, \boldsymbol{x}, \boldsymbol{y}} R_{\mathrm{sec}} \tag{32a}$$

$$\text{s.t. Formulas (12c), (12e), (23), (25)} \tag{32b}$$

$$\text{Formulas (27c), (30), (31)} \tag{32c}$$

$$\boldsymbol{W} \succcurlyeq \mathbf{0} \tag{32d}$$

Problem (32) can be solved by the CVX tool because it is an SDP[17].

For given $\{\boldsymbol{w}, a_K, a_E, v\}$, Problem (27) with optimization variable $\boldsymbol{e}$ can be solved by applying the penalty CCP[14, 18, 19] to relax the unit-modulus constraint (12d). Compared with the SDR technique, the penalty CCP method is capable of finding a feasible solution to meet constraint (12d). In particular, the constraint of Formula (12d) can be relaxed by

$$|e_m^{[j]}|^2 - 2\mathrm{Re}(e_m^{\mathrm{H}} e_m^{[j]}) \leqslant b_m - 1, 1 \leqslant m \leqslant M \tag{33a}$$

$$|e_m|^2 \leqslant 1 + b_{M+m}, 1 \leqslant m \leqslant M \tag{33b}$$

where $e_m^{[j]}$ is any feasible solution, and $\boldsymbol{b} = [b_1, ..., b_{2M}]^{\mathrm{T}}$ are slack vector variables. The proof of Formula (33) can be found in Refs. [14, 18]. Following the penalty CCP framework, the subproblem for optimizing $\boldsymbol{e}$ is thus formulated as follows:

$$\max_{R_{\mathrm{sec}}, \boldsymbol{e}, \boldsymbol{x}, \boldsymbol{y}} R_{\mathrm{sec}} - \lambda^{[j]} \|\boldsymbol{b}\|_1 \tag{34a}$$

$$\text{s.t. Formulas (23), (25), (33)} \tag{34b}$$

Problem (34) is an SDP and can be solved by the CVX tool. The algorithm for finding a feasible solution of $\boldsymbol{e}$ is summarized in Algorithm 1.

In addition, Problem (27) is convex w.r.t. $\{R_{\mathrm{sec}}, v, \boldsymbol{x}, \boldsymbol{y}\}$ for given $\{\boldsymbol{z}, \boldsymbol{w}, \boldsymbol{e}, \boldsymbol{t}, a_K, a_E, \}$, and convex w.r.t. $\{R_{\mathrm{sec}}, a_K, a_E, \boldsymbol{x}, \boldsymbol{y}\}$ for given $\{\boldsymbol{z}, \boldsymbol{w}, \boldsymbol{e}, \boldsymbol{t}, v, \}$. Finally, Problem (27) is addressed under the AO framework containing four subproblems. The convergence of the AO framework can be guaranteed due to the fact that each subproblem can obtain a nondecreasing sequence of objective function values.

Algorithm 1 Penalty CCP optimization for reflection beamforming optimization

Require: Initialize $\boldsymbol{e}^{[0]}$, $\gamma^{[0]} > 1$, and set $j = 0$.
1: **repeat**
2: **if** $j < J_{max}$ **then**
3: Update $\boldsymbol{e}^{[j+1]}$ by solving Problem (34);
4: Update $\lambda^{[j+1]} = \min\{\gamma\lambda^{[j]}, \lambda_{max}\}$;
5: $j = j + 1$;
6: **else**
7: Initialize with a new random $\boldsymbol{e}^{[0]}$, set $\gamma^{[0]} > 1$ again, and set $j = 0$.
8: **end if**
9: **until** $\|\boldsymbol{b}\|_1 \leqslant \chi$ and $\|\boldsymbol{e}^{[j]} - \boldsymbol{e}^{[j-1]}\|_1 \leqslant \nu$.
10: Output $\boldsymbol{e}^{(n+1)} = \boldsymbol{e}^{[j]}$.

4 ED model II: Passive ED model

In this section, we focus on the transmission design for the passive attack, which is more practical and more challenging to address, given that the passive ED can hide itself and its CSI is not known[10, 11]. The authors in Ref. [13] proposed to exploit the angular information of the ED to combat its passive attack, which is also applicable in the current study. In this section, the cascaded LIL channel $\boldsymbol{H}_K$ and the channel $\boldsymbol{H}_{\mathrm{IRS}}$ are assumed to be perfect. This is a reasonable assumption due to the fact that the pilot information for channel estimation for LUs is known at the BS.

4.1 Average eavesdropping rate maximization

The signal received by the ED is formulated as

$$y_E = \boldsymbol{h}_E^{\mathrm{H}} \mathrm{diag}(\boldsymbol{e}^*) \boldsymbol{H}_{\mathrm{IRS}} \boldsymbol{w} s + \sigma_E^2.$$

As the ED is passive, we can only detect the activity of the ED on the line segment between the BS and LU K without knowing its exact location. This detection of a passive attack is based on spectrum sensing[20]. Hence, the average eavesdropping rate is considered which can be computed as follows[13, 21, 22]:

$$R_E^{av}(\boldsymbol{w}, \boldsymbol{e}) = \frac{1}{D_K} \int_0^{D_K} E_{\{\boldsymbol{h}_E\}} \left[\frac{1}{2} \log_2 \left(1 + \frac{1}{\sigma_E^2} \left| \boldsymbol{h}_E^{\mathrm{H}} \mathrm{diag}(\boldsymbol{e}^*) \boldsymbol{H}_{\mathrm{IRS}} \boldsymbol{w} \right|^2 \right) \right] d_{D_E} \tag{35}$$

With Eq. (35), we formulate the following optimization problem:

$$\max_{\boldsymbol{z}, \boldsymbol{w}, \boldsymbol{e}, \boldsymbol{t}} \left\{ \min_{\forall k \in \mathcal{K}} R_k - R_E^{av}(\boldsymbol{w}, \boldsymbol{e}) \right\} \tag{36a}$$

$$\text{s.t. Formulas (12c) − (12f)} \tag{36b}$$

The main challenge in solving Problem (36) is from the average eavesdropping rate containing the integration over D_E and the expectation over $\boldsymbol{h}_E$. To address this issue, we use Jensen's inequality to construct an upper bound of $R_E^{av}(\boldsymbol{w}, \boldsymbol{e})$ given by

$$R_E^{up}(\boldsymbol{w}, \boldsymbol{e}) = \frac{1}{2} \log_2 \left(1 + \frac{\int_0^{D_K} E_{\{\boldsymbol{h}_E\}} \left(\left| \boldsymbol{h}_E^{\mathrm{H}} \mathrm{diag}(\boldsymbol{e}^*) \boldsymbol{H}_{\mathrm{IRS}} \boldsymbol{w} \right|^2 \right) d_{D_E}}{\sigma_E^2 D_K} \right) = \frac{1}{2} \log_2 \left(1 + \frac{1}{\sigma_E^2} \boldsymbol{w}^{\mathrm{H}} \boldsymbol{H}_{\mathrm{IRS}}^{\mathrm{H}} \mathrm{diag}(\boldsymbol{e}) \boldsymbol{R}_E \mathrm{diag}(\boldsymbol{e}^*) \boldsymbol{H}_{\mathrm{IRS}} \boldsymbol{w} \right) \tag{37}$$

where $\boldsymbol{R}_E = \frac{1}{D_K}\int_0^{D_K} E_{\{\boldsymbol{h}_E\}}[\boldsymbol{h}_E\boldsymbol{h}_E^{\mathrm{H}}]d_{D_E}$, which can be computed via one-dimension integration.

According to Eq. (2), we define

$$\overline{\boldsymbol{h}}_E = \sqrt{\varrho_0\left(\frac{d_{\mathrm{IRS},E}}{d_0}\right)^{-\alpha_{\mathrm{IRS}}}\frac{K_{\mathrm{IRS}}}{1+K_{\mathrm{IRS}}}}\boldsymbol{h}_E^{\mathrm{LOS}} \tag{38a}$$

$$\boldsymbol{R}_E = \varrho_0\left(\frac{d_{\mathrm{IRS},E}}{d_0}\right)^{-\alpha_{\mathrm{IRS}}}\frac{1}{1+K_{\mathrm{IRS}}}\boldsymbol{I}_M \tag{38b}$$

where $\overline{\boldsymbol{h}}_E$ describes the LoS component and is the mean of channel $\boldsymbol{h}_E$. Moreover, $\boldsymbol{R}_E$ is a positive semidefinite covariance matrix that represents the non-LoS component's spatial correlation characteristics. Therefore, we have $\boldsymbol{h}_E \sim \mathcal{CN}(\overline{\boldsymbol{h}}_E, \boldsymbol{R}_E)$[23] and further obtain the following:

$$E_{\{\boldsymbol{h}_E\}}[\boldsymbol{h}_E\boldsymbol{h}_E^{\mathrm{H}}] = \left[\boldsymbol{R}_E + \overline{\boldsymbol{h}}_E\overline{\boldsymbol{h}}_E^{\mathrm{H}}\right] = \varrho_0\left(\frac{d_{\mathrm{IRS},E}}{d_0}\right)^{-\alpha_{\mathrm{IRS}}}\cdot \left[\frac{1}{1+K_{\mathrm{IRS}}}\boldsymbol{I}_M + \frac{K_{\mathrm{IRS}}}{1+K_{\mathrm{IRS}}}\boldsymbol{h}_E^{\mathrm{LOS}}(\boldsymbol{h}_E^{\mathrm{LOS}})^{\mathrm{H}}\right].$$

4.2 Proposed algorithm

By replacing $R_E^{av}(\boldsymbol{w},\boldsymbol{e})$ with $R_E^{up}(\boldsymbol{w},\boldsymbol{e})$ in the objective function of Problem (36), we have

$$\max_{\boldsymbol{z},\boldsymbol{w},\boldsymbol{e},\boldsymbol{t}}\left\{\min_{\forall k\in\mathcal{K}} R_k - R_E^{up}\right\} \tag{39a}$$

$$\text{s.t. Formulas (12c)} - \text{(12f)} \tag{39b}$$

Due to the nonconvex constraints and objective function, as well as the coupled variables $\boldsymbol{w}$ and $\boldsymbol{e}$, Problem (39) is still difficult to solve. Hence, we propose an MM-based AO method to update $\boldsymbol{w}$ and $\boldsymbol{e}$ iteratively. Specifically, by first fixing $\boldsymbol{e}$, the nonconcave objective function w.r.t., $\{\boldsymbol{z},\boldsymbol{w},\boldsymbol{t}\}$ is replaced by its customized concave surrogate function and then solved by the CVX. Here, $\{\boldsymbol{z},\boldsymbol{w},\boldsymbol{t}\}$ are fixed, and the closed-form solution of $\boldsymbol{e}$ can be found by constructing an easy-to-solve surrogate objective function w.r.t., $\boldsymbol{e}$.

The surrogate functions of $R_k(z,t_k)$ for $\forall k\in\mathcal{K}_{-K}$ are given by $\widehat{R}_k(z,t_k|z^{(n)},t_k^{(n)}) = \widetilde{R}_k(z,t_k|z^{(n)},t_k^{(n)})$, which is given in Eq. (15). And the surrogate functions of $R_K(\boldsymbol{w},\boldsymbol{e})$ and $R_E(\boldsymbol{w},\boldsymbol{e})$ are given in the following lemma by using the first-order Taylor approximation.

Lemma 6 Assuming that $\{\boldsymbol{w}^{(n)},\boldsymbol{e}^{(n)}\}$ is any feasible solution, then $R_K(\boldsymbol{w},\boldsymbol{e})$ is lower bounded by a concave surrogate function $\widehat{R}_K\left(\boldsymbol{w},\boldsymbol{e}|\boldsymbol{w}^{(n)},\boldsymbol{e}^{(n)}\right)$ defined by

$$\widehat{R}_K(\boldsymbol{w},\boldsymbol{e}|\boldsymbol{w}^{(n)},\boldsymbol{e}^{(n)}) = \frac{1}{2}\log_2\left(1 - \frac{q_K^{(n)}}{\sigma_K^2} + 2\mathrm{Re}\left(\frac{q_K}{\sigma_K^2}\right)\right) \tag{40}$$

where $q_K^{(n)} = \left|\boldsymbol{e}^{(n),\mathrm{H}}\boldsymbol{H}_K\boldsymbol{w}^{(n)}\right|^2$ and $q_K = \boldsymbol{e}^{(n),\mathrm{H}}\boldsymbol{H}_K\boldsymbol{w}^{(n)}\boldsymbol{w}^{\mathrm{H}}\boldsymbol{H}_K^{\mathrm{H}}\boldsymbol{e}$.

Meanwhile, $R_E(\boldsymbol{w},\boldsymbol{e})$ is upper-bounded by a convex surrogate function $\widehat{R}_E\left(\boldsymbol{w},\boldsymbol{e}|\boldsymbol{w}^{(n)},\boldsymbol{e}^{(n)}\right)$ given by

$$\widehat{R}_E^{up}\left(\boldsymbol{w},\boldsymbol{e}|\boldsymbol{w}^{(n)},\boldsymbol{e}^{(n)}\right) = \frac{1}{2}\log_2\left(1+\frac{q_E^{(n)}}{\sigma_E^2}\right) + \frac{q_E - q_E^{(n)}}{2(\sigma_E^2+q_E^{(n)})\ln 2} \tag{41}$$

where $q_E = \boldsymbol{w}^{\mathrm{H}}\boldsymbol{H}_{\mathrm{IRS}}^{\mathrm{H}}\mathrm{diag}(\boldsymbol{e})\boldsymbol{R}_E\mathrm{diag}(\boldsymbol{e}^*)\boldsymbol{H}_{\mathrm{IRS}}\boldsymbol{w}$ and $q_E^{(n)} = \boldsymbol{w}^{(n),\mathrm{H}}\boldsymbol{H}_{\mathrm{IRS}}^{\mathrm{H}}\mathrm{diag}(\boldsymbol{e}^{(n)})\boldsymbol{R}_E\mathrm{diag}((\boldsymbol{e}^{(n)})^*)\boldsymbol{H}_{\mathrm{IRS}}\boldsymbol{w}^{(n)}$.

Furthermore, we have the following proposition.

Proposition 1 The functions $\{\widehat{R}_k,\widehat{R}_K,\widehat{R}_E^{up}\}$ preserve the first-order property of functions $\{R_k,R_K,R_E\}$, respectively. Let us take $\widehat{R}_K$ and R_K as an example.

$$\nabla_{\boldsymbol{w}}\widehat{R}_K(\boldsymbol{w},\boldsymbol{e}^{(n)}|\boldsymbol{w}^{(n)},\boldsymbol{e}^{(n)})|_{\boldsymbol{w}=\boldsymbol{w}^{(n)}} = \nabla_{\boldsymbol{w}}R_K\left(\boldsymbol{w},\boldsymbol{e}^{(n)}\right)|_{\boldsymbol{w}=\boldsymbol{w}^{(n)}},$$
$$\nabla_{\boldsymbol{e}}\widehat{R}_K(\boldsymbol{w}^{(n)},\boldsymbol{e}|\boldsymbol{w}^{(n)},\boldsymbol{e}^{(n)})|_{\boldsymbol{e}=\boldsymbol{e}^{(n)}} = \nabla_{\boldsymbol{e}}R_K\left(\boldsymbol{w}^{(n)},\boldsymbol{e}\right)|_{\boldsymbol{e}=\boldsymbol{e}^{(n)}}.$$

Proof: See Appendix B in Ref. [13].

Giving $\boldsymbol{e}$, by using Eqs. (15), (40), and (41), and Formula (27c), the subproblem of optimizing $\{\boldsymbol{z},\boldsymbol{w},\boldsymbol{t}\}$ is formulated as follows:

$$\max_{\boldsymbol{z},\boldsymbol{w},\boldsymbol{t}}\left\{\min_{\forall k\in\mathcal{K}}\widehat{R}_k - \widehat{R}_E^{up}\right\} \tag{42a}$$

$$\text{s.t. Formulas (12c), (12e), (27c)} \tag{42b}$$

Introducing auxiliary variable r, we can then transform Problem (42) into

$$\max_{\boldsymbol{z},\boldsymbol{w},\boldsymbol{t},r}\left\{r - \widehat{R}_E^{up}\right\} \tag{43a}$$

$$\text{s.t. Formulas (12c), (12e), (27c)} \tag{43b}$$

$$\widehat{R}_k \geqslant r, \forall k\in\mathcal{K} \tag{43c}$$

which is convex and can be solved by using CVX.

Giving $\{\boldsymbol{z},\boldsymbol{w},\boldsymbol{t}\}$ and combining Eqs. (15), (40), and (41), the subproblem w.r.t., $\boldsymbol{e}$ is formulated as follows:

$$\max_{\boldsymbol{e}}\left\{\min_{\forall k\in\mathcal{K}}\widehat{R}_k - \widehat{R}_E^{up}\right\},\ \text{s.t. Formula (12d)} \tag{44}$$

Problem (44) can be solved by transforming it into a second-order cone programming (SOCP) under the

penalty CCP method previously mentioned in Section 3.2. However, the penalty CCP method must first solve a series of SOCP problems, which incurs a high computational complexity. In the following, we aim to derive a low-complexity algorithm containing the closed-form solution of $\boldsymbol{e}$.

Let $\mathcal{R}=\min_{k=1}^{K-1}\{R_k(z,t_k)\}$, which is a constant. Then, Problem (39) is reformulated as

$$\max_{\boldsymbol{e}}\left\{\min\{\mathcal{R},R_K(\boldsymbol{e})\}-R_E^{up}(\boldsymbol{e})\right\},\ \text{s.t. Formula (12d)} \tag{45}$$

for the optimization of $\boldsymbol{e}$.

Before solving Problem (45), we first consider the following two subproblems:

$$\mathcal{P}1:\min_{\boldsymbol{e}} R_E^{up}(\boldsymbol{e}),\ \text{s.t. Formula (12d)}, R_K(\boldsymbol{e})\geqslant\mathcal{R} \tag{46}$$

$$\mathcal{P}2:\max_{\boldsymbol{e}} R_K(\boldsymbol{e})-R_E^{up}(\boldsymbol{e}),\ \text{s.t. Formula (12d)}, R_K(\boldsymbol{e})\leqslant\mathcal{R} \tag{47}$$

Then, we denote the solutions to $\mathcal{P}1$ and $\mathcal{P}2$ as $\boldsymbol{e}_1^{\#}$ and $\boldsymbol{e}_2^{\#}$, respectively. In addition, we denote the objective function value of Problem (45) as $obj(\boldsymbol{e})$, which is a function of $\boldsymbol{e}$. If $obj(\boldsymbol{e}_1^{\#})\geqslant obj(\boldsymbol{e}_2^{\#})$, then the optimal solution of Problem (45) is given by $\boldsymbol{e}_1^{\#}$. Otherwise, the optimal solution is $\boldsymbol{e}_2^{\#}$. The following lemma shows the solutions of Problem $\mathcal{P}1$.

Lemma 7 The optimal solution of $\mathcal{P}1$ is given by

$$\boldsymbol{e}_1^{\#}=\exp\{\mathrm{j}\arg((\lambda_{\max}(\boldsymbol{A}_E)\boldsymbol{I}-\boldsymbol{A}_E+\varrho_1^{opt}\boldsymbol{A}_K)\boldsymbol{e}^{(n)})\} \tag{48}$$

where $\boldsymbol{A}_E=(\boldsymbol{H}_{\mathrm{IRS}}\boldsymbol{w}\boldsymbol{w}^{\mathrm{H}}\boldsymbol{H}_{\mathrm{IRS}}^{\mathrm{H}})\odot(\boldsymbol{R}_E^{\mathrm{T}}/\sigma_E^2)$, $\boldsymbol{A}_K=\boldsymbol{H}_K\boldsymbol{w}\boldsymbol{w}^{\mathrm{H}}\boldsymbol{H}_K^{\mathrm{H}}/\sigma_K^2$, and ϱ_1^{opt} is the price introduced by the price mechanism[24].

The optimal solution of $\mathcal{P}2$ is given by

$$\boldsymbol{e}_2^{\#}=\exp\{\mathrm{j}\arg(\boldsymbol{c}+\varrho_2^{opt}(\lambda_{\max}(\boldsymbol{A}_K)\boldsymbol{I}-\boldsymbol{A}_K)\boldsymbol{e}^{(n)})\} \tag{49}$$

where ϱ_2^{opt} is the price and

$$\boldsymbol{c}=\frac{1+d_K^{(n)}}{(1+d_E^{(n)})^2}(\lambda_{\max}(\boldsymbol{A}_E)\boldsymbol{I}-\boldsymbol{A}_E)\boldsymbol{e}^{(n)}+\frac{\boldsymbol{A}_K\boldsymbol{e}^{(n)}}{1+d_E^{(n)}},$$
$$d_K^{(n)}=\boldsymbol{e}^{(n),\mathrm{H}}\boldsymbol{A}_K\boldsymbol{e}^{(n)},d_E^{(n)}=\boldsymbol{e}^{(n),\mathrm{H}}\boldsymbol{A}_E\boldsymbol{e}^{(n)}.$$

Proof: See Appendix C.

Given that $\boldsymbol{e}_1^{\#}$ and $\boldsymbol{e}_2^{\#}$ are the globally optimal solutions of $\mathcal{P}1$ and $\mathcal{P}2$, respectively; hence, $\boldsymbol{e}^{\#}$ is the globally optimal solution of Problem (45). The optimal price parameter can be obtained by using the bisection search method detailed in Ref. [24].

According to Proposition 1 and Theorem 1 in Ref. [25], the sequence $\{\boldsymbol{z}^{(n)},\boldsymbol{w}^{(n)},\boldsymbol{t}^{(n)},\boldsymbol{e}^{(n)}\}_{n=1,2,3,\ldots}$ obtained in each iteration is guaranteed to converge to the set of stationary points of Problem (39). The computational complexity of Problem (43) mainly comes from second-order cone (SOC) constraints and is given by $O(\sqrt{2I}(n^3+n^2\sum_{i=1}^{I}a_i^2))$, where I and n refer to the number of SOC of size a_i and the number of variables, respectively[14]. Thus, the computational complexity of Problem (43) is $O(\sqrt{2N}(n^3+n^2((N-1)^2+K-1)))$, where $n=N+2K-3$. The computational complexity of Eq. (48) or Eq. (49) mainly comes from the eigenvalue operation, whose complexity is $O(N^3)$. Therefore, the total complexity of solving Problem (39) at each iteration is given by $O(\sqrt{2N}(n^3+n^2((N-1)^2+K-1)+N^3))$.

5 Numerical results and discussions

This section illustrates the performances of the proposed schemes and algorithms in terms of the secrecy rate, the feasibility rate, and complexity. The results are obtained by using a computer with a 1.99 GHz i7-8550U CPU and 16 GB RAM. A polar coordinate system is used to describe the simulated system setup: the BS is located at (0 m, 0 m), and the IRS is placed at (50 m, 0 m) with elevation angle $\phi=\frac{2\pi}{3}$; K LUs are randomly and uniformly distributed in an area with $D_k\sim\mathcal{U}(20\text{ m},40\text{ m})$ and $\theta_k\sim\mathcal{U}(-\frac{\pi}{2},\frac{\pi}{2})$ for $\forall k\in\mathcal{K}$, where $\mathcal{U}$ is the uniform distribution. The ED is located at (D_E,θ_K) with $D_E\in(0,D_K)$. The pathloss at the distance of 1 m is −30 dB, the pathloss exponents are set to $\alpha_{\mathrm{BS}}=\alpha_{\mathrm{IRS}}=2.2$, and the Rician factor is 5. The transmit power budget at the BS is set to $P_{\max}=$ 30 dBm, and the noise powers are $\{\sigma_i^2=-90\text{ dBm}\}_{\forall i\in\mathcal{K}_{+E}}$. For the statistical CSI error model, the variances of $\{\Delta_i^K,\Delta_i^E\}_{\forall i\in\mathcal{K}_{-K}}$ are defined as $\{\varepsilon_{K,i}^2=\delta_K^2\|\boldsymbol{h}_K^*\odot\boldsymbol{h}_i\|_2^2,\varepsilon_{E,i}^2=\delta_E^2\|\boldsymbol{h}_E^*\odot\boldsymbol{h}_i\|_2^2\}_{\forall i\in\mathcal{K}_{-K}}$, where $\delta_K\in[0,1)$ and $\delta_E\in[0,1)$ measure the relative amounts of CSI uncertainties. In addition, the outage probability of secrecy rate is $\rho=0.05$.

5.1 Robust secrecy rate in ED model I

The cases of $N=8$ and $K=5$ are simulated to verify the performance of the proposed outage-constrained

beamforming in the user cooperation systems. For comparison, we also consider the "Non-robust" as the benchmark scheme, in which the estimated cascaded LIL and LIE channels are naively regarded as perfect channels, resulting in the following problem:

$$\max_{\boldsymbol{z},\boldsymbol{w},\boldsymbol{e},t}\left\{\min_{\forall k\in\mathcal{K}} R_k - R_E\right\} \tag{50a}$$

$$\text{s.t. Formulas (12c)} - \text{(12f)} \tag{50b}$$

where $R_K(\boldsymbol{e}) = \frac{1}{2}\log_2(1+|\boldsymbol{e}^{\mathrm{H}}\widehat{\boldsymbol{H}}_K\boldsymbol{w}|^2/\sigma_K^2)$ and $R_E(\boldsymbol{e}) = \frac{1}{2}\log_2(1+|\boldsymbol{e}^{\mathrm{H}}\widehat{\boldsymbol{H}}_E\boldsymbol{w}|^2/\sigma_E^2)$. Thus, Problem (50) can be solved by using the proposed low-complexity algorithm used to solve Problem (36).

Figure 3 investigates the feasibility rate and the maximum secrecy rate versus the distance of the ED, in which the coordinate of the X-axis is set to the ratio of D_E/D_K. The "feasibility rate" is defined as the ratio of the number of channel realizations that have a feasible solution to the outage-constrained problem of Formula (12) to the total number of channel realizations. As shown in Fig. 3a, that the closer the ED is to LU K, the lower the feasibility rate will be, indicating that the location of the ED imposes a great threat to the security system. From Fig. 3b, we can also see that the secrecy rate drops fast when the ED approaches LU K, and this is reduced to zero when the channel error is large. In this situation, the whole system is no longer suitable for secure communication.

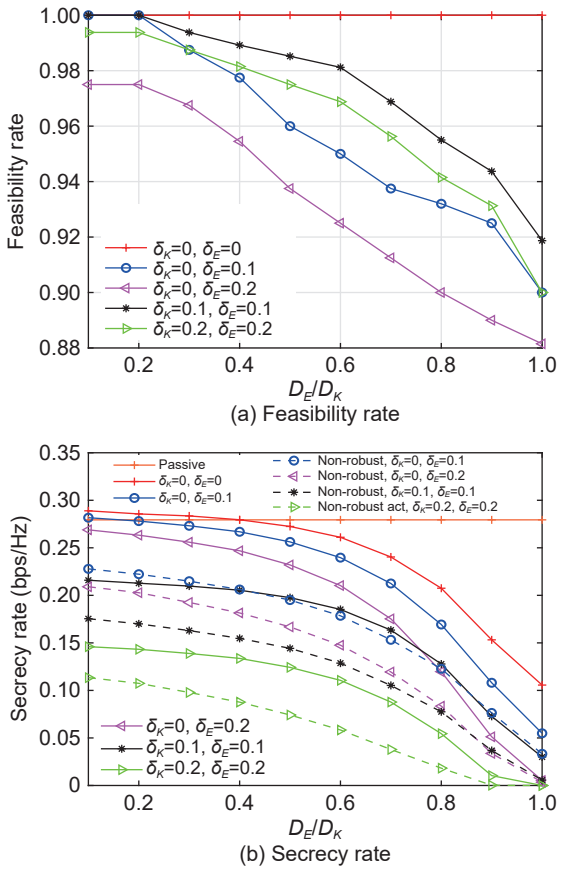

Fig. 3 Feasibility rate and secrecy rate versus D_E/D_K under $N=8$, $M=32$, and $K=5$.

Next, the performance versus the size of the IRS, i.e., M, is verified in Fig. 4. Let us assume that the ED is located at $D_E/D_K = 0.5$. In Fig. 4, the case of $\delta_K = \delta_E = 0$ is regarded as the perfect cascaded CSI case, and its maximum secrecy rate increases with M, which is consistent with that of Fig. 6 in Ref. [12]. The performance of $\delta_K = \delta_E = 0$ can be used as the performance upper bound of the proposed outage-constrained beamforming method. Furthermore, the maximum secrecy rate is obviously degraded with enlarged channel uncertainty levels. Moreover, it is observed that black line of $\{\delta_K = 0.2, \delta_E = 0\}$ outperforms the pink line of $\{\delta_K = 0, \delta_E = 0.2\}$. This indicates that the negative impact of cascaded LIL channel error on secrecy rate is higher than that of the cascaded LIE channel error.

5.2 Average secrecy rate in ED model II

This subsection evaluates the performance of the proposed scheme under the passive attack mode. In order to evaluate the performance of the proposed low-complexity algorithm, we consider two benchmark algorithms given by: (1) the "SOCP" scheme, in which

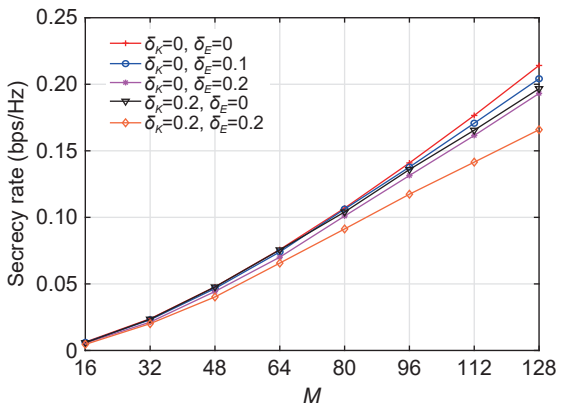

Fig. 4 Secrecy rate versus M under $N=8$ and $K=5$.

the CVX tool is used to solve the SOCP version of Problem (44), and (2) the "Random" scheme, in which the phases of the reflecting elements are randomly generated.

Figure 5 illustrates the respective outcomes in terms of the average secrecy rate and the computational complexity under the system settings of $N = 8$ and $K = 5$. As can be seen in Fig. 5a, the proposed algorithm with a semi-closed-form solution is almost the same as that of the SOCP-based algorithm with global optimal solution, and both of them outperform the scheme with random reflecting phases. Moreover, increasing the number of reflecting elements at the IRS can significantly enhance the average secrecy rate of the system. Figure 5b describes the CPU time consumption required for these three algorithms to evaluate the computational complexity of the algorithms. It can be seen that the proposed algorithm with a closed-form solution requires much less CPU running time than the SOCP-based scheme. In addition, the CPU running time of the SCOP-based algorithm is scaled with M, while the proposed algorithm is not sensitive to M. This is due to the fact that the computational complexity of the SOCP depends on M, while that of the closed-form solution does not.

Finally, Fig. 6 illustrates the performance versus the number of users when $M = 64$. Thus, we can obtain the same conclusion as above: The proposed algorithm has the same performance as the SOCP-based algorithm but consumes less CPU running time.

6 Conclusion

In this work, we have proposed a two-phase IRS-aided communication system with the aim of realizing secure communication under the scenarios of active attacks and passive eavesdropping. We addressed the cascaded channel error caused by the active attacks by maximizing the secrecy rate subject to secrecy rate

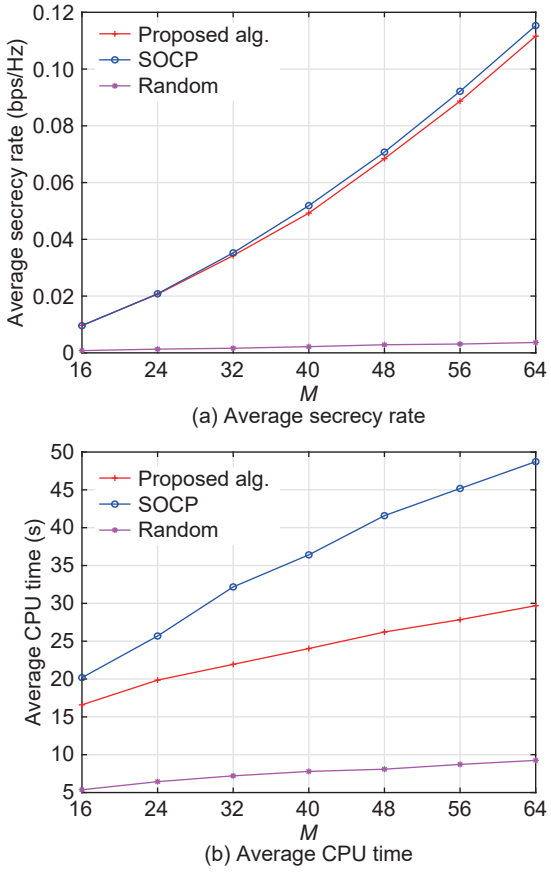

Fig. 5 Average secrecy rate and CPU time versus M under $N = 8$ and $K = 5$.

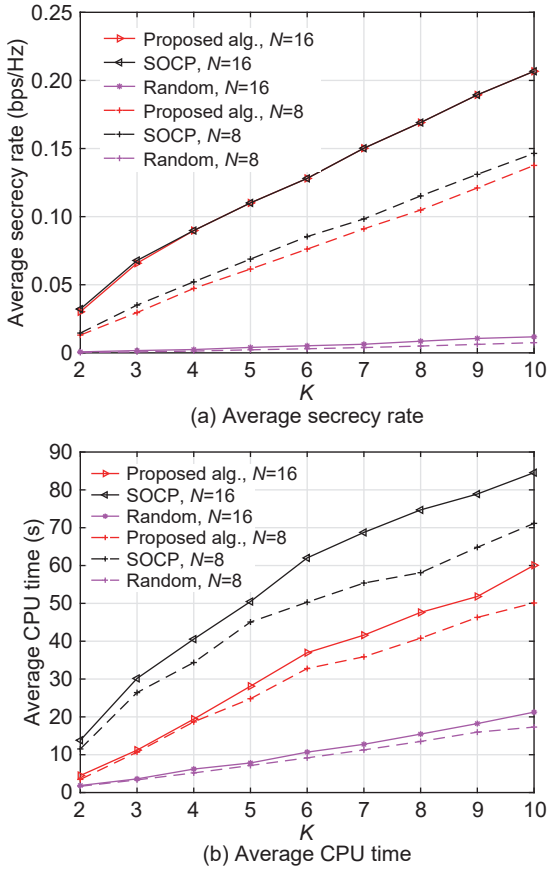

Fig. 6 Average secrecy rate and CPU time versus K under $M = 64$.

outage probability constraints, which has been tackled by using the BTI. For the case of the partial CSI of the ED, the average secrecy rate maximization problem was considered, which is addressed by the proposed low-complexity algorithm. It has been shown that the negative effect of the ED's channel error is greater than that of the LU. In addition, when the channel error is large, the number of elements on the IRS has a negative impact on system performance. This conclusion provides an engineering-derived insight for the careful selection of the number of elements at the IRS.

Appendix

A Proof of Lemma 2

To begin, we introduce the following lemma.

Lemma A1 Assuming that $x \geqslant 0$ is a positive real number, and considering the function $g_1(a,x) = -ax + \ln a + 1$, we thus have

$$\ln x^{-1} = \max_{a \geqslant 0} g_1(a,x).$$

By applying Lemma A1, we can construct an upper bound of rate $R_E(\boldsymbol{w},\boldsymbol{e})$ as follows:

$$\begin{aligned}
&R_E(\boldsymbol{w},\boldsymbol{e}) = \\
&\frac{-\ln(1+\left|\boldsymbol{e}^{\mathrm{H}}\boldsymbol{H}_E\boldsymbol{w}\right|^2/\sigma_E^2)^{-1}}{2\ln 2} \overset{\text{(a)}}{=} \\
&\frac{-\max_{a_E \geqslant 0} g_1(a_E, 1+\left|\boldsymbol{e}^{\mathrm{H}}\boldsymbol{H}_E\boldsymbol{w}\right|^2/\sigma_E^2)}{2\ln 2} = \\
&\frac{\min_{a_E \geqslant 0} -g_1(a_E, 1+\left|\boldsymbol{e}^{\mathrm{H}}\boldsymbol{H}_E\boldsymbol{w}\right|^2/\sigma_E^2)}{2\ln 2} \leqslant \\
&\frac{-g_1(a_E, 1+\left|\boldsymbol{e}^{\mathrm{H}}\boldsymbol{H}_E\boldsymbol{w}\right|^2/\sigma_E^2)}{2\ln 2}, \text{ for any } a_E \geqslant 0 = \\
&\frac{a_E\left|\boldsymbol{e}^{\mathrm{H}}\boldsymbol{H}_E\boldsymbol{w}\right|^2/\sigma_E^2 + a_E - \ln a_E - 1}{2\ln 2} = \\
&\widetilde{R}_E(\boldsymbol{w},\boldsymbol{e},a_E)
\end{aligned} \tag{A1}$$

where Eq. (A1a) is from Lemma A1.

Hence, the proof is completed.

B Proof of Lemma 3

To prove Lemma 3, we first introduce the following lemma.

Lemma A2 Assuming that v is a complex number and considering the function $g_2(v,x) = (|x|^2+\sigma^2)|v|^2 - 2\mathrm{Re}(vx) + 1$, we thus have

$$\frac{\sigma^2}{|x|^2+\sigma^2} = \min_v g_2(a,x).$$

By applying Lemma A2, we can construct a lower bound of rate $R_K(\boldsymbol{w},\boldsymbol{e})$ as follows:

$$\begin{aligned}
&R_K(\boldsymbol{w},\boldsymbol{e}) = \\
&\frac{\ln\left(1-\frac{|\boldsymbol{e}^{\mathrm{H}}\boldsymbol{H}_K\boldsymbol{w}|^2}{\sigma_K^2+|\boldsymbol{e}^{\mathrm{H}}\boldsymbol{H}_K\boldsymbol{w}|^2}\right)^{-1}}{2\ln 2} \overset{\text{(a)}}{=} \\
&\frac{\max_{a_K \geqslant 0} g(a_K, 1-\frac{|\boldsymbol{e}^{\mathrm{H}}\boldsymbol{H}_K\boldsymbol{w}|^2}{\sigma_K^2+|\boldsymbol{e}^{\mathrm{H}}\boldsymbol{H}_K\boldsymbol{w}|^2})}{2\ln 2} \geqslant \\
&\frac{g(a_K, 1-\frac{|\boldsymbol{e}^{\mathrm{H}}\boldsymbol{H}_K\boldsymbol{w}|^2}{\sigma_K^2+|\boldsymbol{e}^{\mathrm{H}}\boldsymbol{H}_K\boldsymbol{w}|^2})}{2\ln 2}, \text{ for any } a_K \geqslant 0 = \\
&\frac{-a_K\left(\frac{\sigma_K^2}{\sigma_K^2+|\boldsymbol{e}^{\mathrm{H}}\boldsymbol{H}_K\boldsymbol{w}|^2}\right)+\ln a_K+1}{2\ln 2} \overset{\text{(b)}}{=} \\
&\frac{-a_K\left(\min_v g_2(v,\boldsymbol{e}^{\mathrm{H}}\boldsymbol{H}_K\boldsymbol{w})\right)+\ln a_K+1}{2\ln 2} = \\
&\frac{a_K\left(\max_v -g_2(v,\boldsymbol{e}^{\mathrm{H}}\boldsymbol{H}_K\boldsymbol{w})\right)+\ln a_K+1}{2\ln 2} \geqslant \\
&\frac{a_K\left(-g_2(v,\boldsymbol{e}^{\mathrm{H}}\boldsymbol{H}_K\boldsymbol{w})\right)+\ln a_K+1}{2\ln 2}, \text{ for any } v \geqslant 0 = \\
&\frac{1}{2\ln 2}(-a_K|v|^2|\boldsymbol{e}^{\mathrm{H}}\boldsymbol{H}_K\boldsymbol{w}|^2 - \sigma_K^2 a_K|v|^2 + \\
&\quad 2a_K\mathrm{Re}\left(v\boldsymbol{e}^{\mathrm{H}}\boldsymbol{H}_K\boldsymbol{w}\right) - a_K + \ln a_K + 1) = \\
&\widetilde{R}_K(\boldsymbol{w},\boldsymbol{e},a_K,v)
\end{aligned} \tag{A2}$$

where Eq. (A2a) is from Lemma A1, and Eq. (A2b) is from Lemma A2.

Hence, the proof is completed.

C Proof of Lemma 7

To begin with, we solve $\mathcal{P}1$: $\mathcal{P}1$, which is equivalent to

$$\min_{\boldsymbol{e}} \ \boldsymbol{e}^{\mathrm{H}}\boldsymbol{A}_E\boldsymbol{e} \tag{A3a}$$

$$\text{s.t. Formula (12d)} \tag{A3b}$$

$$\boldsymbol{e}^{\mathrm{H}}\boldsymbol{A}_K\boldsymbol{e} \geqslant e^{2\mathcal{R}} - 1 \tag{A3c}$$

Step 1 Construct a surrogate problem.

Under the MM algorithm framework[26], we have the following lemma.

Lemma A3[27, 28] Given $\boldsymbol{A} \succcurlyeq \boldsymbol{A}_0$ and $\boldsymbol{x}$, then the quadratic function $\boldsymbol{x}^{\mathrm{H}}\boldsymbol{A}_0\boldsymbol{x}$ is majorized by

$\boldsymbol{x}^{\mathrm{H}}\boldsymbol{A}\boldsymbol{x}-2\mathrm{Re}(\boldsymbol{x}^{(n),\mathrm{H}}(\boldsymbol{A}-\boldsymbol{A}_0)\boldsymbol{x})+\boldsymbol{x}^{(n),\mathrm{H}}(\boldsymbol{A}-\boldsymbol{A}_0)\boldsymbol{x}^{(n)}$ at $\boldsymbol{x}^{(n)}$.

By adopting Lemma A3 and setting $\boldsymbol{A}=\lambda_{\max}(\boldsymbol{A}_E)\boldsymbol{I}$ for simplicity, the quadratic objective function in Formula (A3a) is majorized by

$$2\lambda_{\max}(\boldsymbol{A}_E)M-2\mathrm{Re}(\boldsymbol{e}^{(n),\mathrm{H}}(\lambda_{\max}(\boldsymbol{A}_E)\boldsymbol{I}-\boldsymbol{A}_E)\boldsymbol{e})-\boldsymbol{e}^{(n),\mathrm{H}}\boldsymbol{A}_E\boldsymbol{e}^{(n)} \tag{A4}$$

at a feasible point $\boldsymbol{e}^{(n)}$. Then, we replace $\boldsymbol{e}^{\mathrm{H}}\boldsymbol{A}_K\boldsymbol{e}$ with its linear lower bound to deal with the nonconvex constraint (A3c), thus resulting in the following equivalent constraint:

$$\text{Formula (A3c)} \Rightarrow 2\mathrm{Re}(\boldsymbol{e}^{(n),\mathrm{H}}\boldsymbol{A}_K\boldsymbol{e})\geqslant e^{2\mathcal{R}}-1+\boldsymbol{e}^{(n),\mathrm{H}}\boldsymbol{A}_K\boldsymbol{e}^{(n)} \tag{A5}$$

Step 2 Closed-form solution.

By omitting the constant, Problem (A3) then becomes

$$\max_{\boldsymbol{e}}\ 2\mathrm{Re}(\boldsymbol{e}^{(n),\mathrm{H}}(\lambda_{\max}(\boldsymbol{A}_E)\boldsymbol{I}-\boldsymbol{A}_E)\boldsymbol{e}) \tag{A6a}$$

$$\text{s.t. Formulas (12d), (A5)} \tag{A6b}$$

We introduce a price mechanism for solving Problem (A6) according to Ref. [24], in which ϱ_1 is a nonnegative price:

$$\max_{\boldsymbol{e}}\ 2\,\mathrm{Re}(\boldsymbol{e}^{(n),\mathrm{H}}(\lambda_{\max}(\boldsymbol{A}_E)\boldsymbol{I}-\boldsymbol{A}_E)\boldsymbol{e})+\varrho_1 2\mathrm{Re}(\boldsymbol{e}^{(n),\mathrm{H}}\boldsymbol{A}_K\boldsymbol{e})$$
$$\text{s.t. Formula (12d).}$$

Then, the globally optimal solution is given by

$$\boldsymbol{e}_1^{\#}(\varrho_1^{opt})=\exp\{\mathrm{j}\arg((\lambda_{\max}(\boldsymbol{A}_E)\boldsymbol{I}-\boldsymbol{A}_E+\varrho_1\boldsymbol{A}_K)\boldsymbol{e}^{(n)})\}.$$

The optimal ϱ_1^{opt} is determined by using the bisection search method. The detailed information about this can be found in Ref. [24].

Then, we solve $\mathcal{P}2$: $\mathcal{P}2$, which is equivalent to

$$\max_{\boldsymbol{e}}\ \frac{1+\boldsymbol{e}^{\mathrm{H}}\boldsymbol{A}_K\boldsymbol{e}}{1+\boldsymbol{e}^{\mathrm{H}}\boldsymbol{A}_E\boldsymbol{e}} \tag{A7a}$$

$$\text{s.t. Formula (12d)} \tag{A7b}$$

$$\boldsymbol{e}^{\mathrm{H}}\boldsymbol{A}_K\boldsymbol{e}\leqslant e^{2\mathcal{R}}-1 \tag{A7c}$$

Step 1 Construct a surrogate problem.

Under the MM algorithm framework, we construct a linear lower bound of the objective function in Formula (A7a) as follows:

$$\frac{1+\boldsymbol{e}^{\mathrm{H}}\boldsymbol{A}_K\boldsymbol{e}}{1+\boldsymbol{e}^{\mathrm{H}}\boldsymbol{A}_E\boldsymbol{e}}\overset{\text{(a)}}{\geqslant}\frac{2\mathrm{Re}(1+d_K)}{1+d_E^{(n)}}-\frac{1+d_K^{(n)}}{(1+d_E^{(n)})^2}\left(1+\boldsymbol{e}^{\mathrm{H}}\boldsymbol{A}_E\boldsymbol{e}\right)\overset{\text{(b)}}{\geqslant}\frac{2\mathrm{Re}(1+d_K)}{1+d_E^{(n)}}-\frac{1+d_K^{(n)}}{(1+d_E^{(n)})^2}-\frac{1+d_K^{(n)}}{(1+d_E^{(n)})^2}\cdot(2\lambda_{\max}(\boldsymbol{A}_E)M-2\mathrm{Re}(\boldsymbol{e}^{(n),\mathrm{H}}(\lambda_{\max}(\boldsymbol{A}_E)\boldsymbol{I}-\boldsymbol{A}_E)\boldsymbol{e})-d_E^{(n)})=2\mathrm{Re}(\boldsymbol{c}^{\mathrm{H}}\boldsymbol{e})+\text{const},$$

where $d_K=\boldsymbol{e}^{(n),\mathrm{H}}\boldsymbol{A}_K\boldsymbol{e}$. $\{d_K^{(n)},d_E^{(n)},\boldsymbol{c}\}$ are defined in Lemma 7, and Formulas (a) and (b) are from Lemma 1 and Lemma A3, respectively. By using Lemma A3 again, the convex constraint (A7c) can be replaced by an easy-to-solve form as

$$\text{Formula (A7c)} \Rightarrow 2\mathrm{Re}(\boldsymbol{e}^{(n),\mathrm{H}}(\lambda_{\max}(\boldsymbol{A}_K)\boldsymbol{I}-\boldsymbol{A}_K)\boldsymbol{e})\geqslant -2\lambda_{\max}(\boldsymbol{A}_K)M-e^{2\mathcal{R}}+1-\boldsymbol{e}^{(n),\mathrm{H}}\boldsymbol{A}_K\boldsymbol{e}^{(n)} \tag{A8}$$

Step 2 Closed-form solution.

By omitting the constant, Problem (A7) is then equivalent to

$$\max_{\mathbf{e}}\ 2\mathrm{Re}(\boldsymbol{c}^{\mathrm{H}}\boldsymbol{e}) \tag{A9a}$$

$$\text{s.t. Formulas (12d), (A8)} \tag{A9b}$$

By using the price mechanism, Problem (A7) is reformulated as follows:

$$\max_{\boldsymbol{e}}\ 2\mathrm{Re}(\boldsymbol{c}^{\mathrm{H}}\boldsymbol{e})+\varrho_2 2\mathrm{Re}(\boldsymbol{e}^{(n),\mathrm{H}}(\lambda_{\max}(\boldsymbol{A}_K)\boldsymbol{I}-\boldsymbol{A}_K)\boldsymbol{e}),$$
$$\text{s.t. Formula (12d).}$$

where ϱ_2 is a nonnegative price. The globally optimal solution is given by $\boldsymbol{e}_2^{\#}(\varrho_2^{opt})=\exp\{\mathrm{j}\arg(\boldsymbol{c}+\varrho_2(\lambda_{\max}(\boldsymbol{A}_K)\boldsymbol{I}-\boldsymbol{A}_K)\boldsymbol{e}^{(n)})\}$, where the optimal ϱ_2^{opt} is determined by using the bisection search method.

Therefore, the proof is completed.

References

[1] G. Zhou, C. Pan, H. Ren, K. Zhi, S. Hong, and K. K. Chai, User cooperation for RIS-aided secure SWIPT MIMO systems under the passive eavesdropping, in *Proc. 2021 IEEE/CIC International Conference on Communications in China (ICCC Workshops)*, Xiamen, China, 2021, pp. 171–176.

[2] E. Basar, M. Di Renzo, J. De Rosny, M. Debbah, M. -S. Alouini, and R. Zhang, Wireless communications through reconfigurable intelligent surfaces, *IEEE Access*, vol. 7, pp. 116753–116773, 2019.

[3] M. Di Renzo, K. Ntontin, J. Song, F. Danufane, X. Qian,

F. Lazarakis, J. De Rosny, D. -T. Phan-Huy, O. Simeone, R. Zhang, et al., Reconfigurable intelligent surfaces vs. relaying: Differences, similarities, and performance comparison, *IEEE Open Journal of the Communications Society*, vol. 1, pp. 798–807, 2020.

[4] K. -K. Wong, K. -F. Tong, Z. Chu, and Y. Zhang, A vision to smart radio environment: Surface wave communication superhighways, *IEEE Wireless Communications*, vol. 28, no. 1, pp. 112–119, 2021.

[5] H. Shen, W. Xu, S. Gong, Z. He, and C. Zhao, Secrecy rate maximization for intelligent reflecting surface assisted multi-antenna communications, *IEEE Commun. Lett.*, vol. 23, no. 9, pp. 1488–1492, 2019.

[6] S. Hong, C. Pan, H. Ren, K. Wang, and A. Nallanathan, Artificial-noise-aided secure MIMO wireless communications via intelligent reflecting surface, *IEEE Trans. Commun.*, vol. 68, no. 12, pp. 7851–7866, 2020.

[7] X. Guan, Q. Wu, and R. Zhang, Intelligent reflecting surface assisted secrecy communication: Is artificial noise helpful or not? *IEEE Wireless Communications Letters*, vol. 9, no. 6, pp. 778–782, 2020.

[8] X. Yu, D. Xu, Y. Sun, D. W. K. Ng, and R. Schober, Robust and secure wireless communications via intelligent reflecting surfaces, *IEEE Journal on Selected Areas in Communications*, vol. 38, no. 11, pp. 2637–2652, 2020.

[9] S. Hong, C. Pan, H. Ren, K. Wang, K. K. Chai, and A. Nallanathan, Robust transmission design for intelligent reflecting surface aided secure communication systems with imperfect cascaded CSI, *IEEE Trans. Wireless Commun.*, vol. 20, no. 4, pp. 2487–2501, 2021.

[10] D. Kapetanovic, G. Zheng, and F. Rusek, Physical layer security for massive MIMO: An overview on passive eavesdropping and active attacks, *IEEE Commun. Mag.*, vol. 53, no. 6, pp. 21–27, 2015.

[11] Y. Wu, A. Khisti, C. Xiao, G. Caire, K. Wong, and X. Gao, A survey of physical layer security techniques for 5G wireless networks and challenges ahead, *IEEE J. Sel. Areas Commun.*, vol. 36, no. 4, pp. 679–695, 2018.

[12] G. Zhou, C. Pan, H. Ren, K. Wang, and A. Nallanathan, Intelligent reflecting surface aided multigroup multicast MISO communication systems, *IEEE Trans. Signal Process.*, vol. 68, pp. 3236–3251, 2020.

[13] S. Wang, M. Wen, M. Xia, R. Wang, Q. Hao, and Y. -C. Wu, Angle aware user cooperation for secure massive MIMO in Rician fading channel, *IEEE J. Sel. Areas Commun.*, vol. 38, no. 9, pp. 2182–2196, 2020.

[14] G. Zhou, C. Pan, H. Ren, K. Wang, and A. Nallanathan, A framework of robust transmission design for IRS-aided MISO communications with imperfect cascaded channels, *IEEE Trans. Signal Process.*, vol. 68, pp. 5092–5106, 2020.

[15] S. Boyd and L. Vandenberghe, *Convex Optimization*. Cambridge, UK: Cambridge Univ. Press, 2004.

[16] I. Bechar, A bernstein-type inequality for stochastic processes of quadratic forms of Gaussian variables, https://arxiv.org/abs/0909.3595, 2009.

[17] M. Grant and S. Boyd, CVX: Matlab software for disciplined convex programming, Version 2.2. http://cvxr.com/cvx, 2020.

[18] G. Zhou, C. Pan, H. Ren, K. Wang, M. Di Renzo, and A. Nallanathan, Robust beamforming design for intelligent reflecting surface aided MISO communication systems, *IEEE Wireless Commun. Lett.*, vol. 9, no. 10, pp. 1658–1662, 2020.

[19] T. Lipp and S. Boyd, Variations and extension of the convex-concave procedure, *Optim. Eng.*, vol. 17, no. 2, pp. 263–287, 2016.

[20] A. Chaman, J. Wang, J. Sun, H. Hassanieh, and R. R. Choudhury, Ghostbuster: Detecting the presence of hidden eavesdroppers, in *Proc. 24th Annual International Conference on Mobile Computing and Networking*, New Delhi, India, 2018, pp. 337–351.

[21] A. Mukherjee, Physical-layer security in the internet of things: Sensing and communication confidentiality under resource constraints, *Proc. IEEE*, vol. 103, no. 10, pp. 1747–1761, 2015.

[22] L. Mucchi, L. Ronga, X. Zhou, K. Huang, Y. Chen, and R. Wang, A new metric for measuring the security of an environment: The secrecy pressure, *IEEE Trans. Wireless Commun.*, vol. 16, no. 5, pp. 3416–3430, 2017.

[23] Ö. Özdogan, E. Björnson, and E. G. Larsson, Massive MIMO with spatially correlated Rician fading channels, *IEEE Trans. Commun.*, vol. 67, no. 5, pp. 3234–3250, 2019.

[24] C. Pan, H. Ren, K. Wang, M. Elkashlan, A. Nallanathan, J. Wang, and L. Hanzo, Intelligent reflecting surface aided MIMO broadcasting for simultaneous wireless information and power transfer, *IEEE J. Sel. Areas Commun.*, vol. 38, no. 8, pp. 1719–1734, 2020.

[25] B. R. Marks and G. P. Wright, Technical note—A general inner approximation algorithm for nonconvex mathematical programs, *Operation Research*, vol. 26, no. 4, pp. 681–683, 1978.

[26] Y. Sun, P. Babu, and D. P. Palomar, Majorization-minimization algorithms in signal processing, communications, and machine learning, *IEEE Trans. Signal Process.*, vol. 65, no. 3, pp. 794–816, 2017.

[27] J. Song, P. Babu, and D. P. Palomar, Optimization methods for designing sequences with low autocorrelation sidelobes, *IEEE Trans. Signal Process.*, vol. 63, no. 15, pp. 3998–4009, 2015.

[28] C. Pan, H. Ren, K. Wang, W. Xu, M. Elkashlan, A. Nallanathan, and L. Hanzo, Multicell MIMO communications relying on intelligent reflecting surfaces, *IEEE Trans. Wireless Commun.*, vol. 19, no. 8, pp. 5218–5233, 2020.

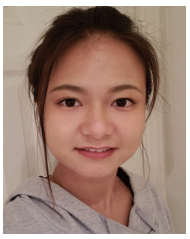

Gui Zhou received the BS and ME degrees from Beijing Institute of Technology, Beijing, China, in 2015 and 2019, respectively. She is currently pursuing the PhD degree at the School of Electronic Engineering and Computer Science, Queen Mary University of London, UK. Her major research interests include intelligent reflection surface (IRS) and signal processing.

Cunhua Pan received the BS and PhD degrees from Southeast University, Nanjing, China, in 2010 and 2015, respectively. From 2015 to 2016, he was a research associate at the University of Kent, UK. He held a postdoctoral position at Queen Mary University of London, UK, from 2016 and 2019. From 2019 to 2021, he was a lecturer in the same university. From 2021, he has been a full professor in Southeast University. His research interests mainly include reconfigurable intelligent surfaces (RIS), intelligent reflection surface (IRS), ultra-reliable low latency communication (URLLC), machine learning, UAV, Internet of Things, and mobile edge computing. He is currently an editor of *IEEE Wireless Communication Letters*, *IEEE Communications Letters*, and *IEEE Access*. He serves as the guest editor for *IEEE Journal on Selected Areas in Communications* on the special issue on xURLLC in 6G: Next generation ultra-reliable and low-latency communications. He also serves as a leading guest editor of *IEEE Journal of Selected Topics in Signal Processing (JSTSP)* special issue on advanced signal processing for reconfigurable intelligent surface-aided 6G networks, *IEEE Vehicular Technology Magazine* on the special issue on backscatter and reconfigurable intelligent surface empowered wireless communications in 6G, and *IEEE Open Journal of Vehicular Technology* on the special issue of reconfigurable intelligent surface empowered wireless communications in 6G and beyond.

Hong Ren received the BS degree in electrical engineering from Southwest Jiaotong University, Chengdu, China, in 2011, and the MS and PhD degrees in electrical engineering from Southeast University, Nanjing, China, in 2014 and 2018, respectively. From 2016 to 2018, she was a visiting student with the School of Electronics and Computer Science, University of Southampton, UK. From 2018 to 2020, she was a postdoctoral researcher with the Queen Mary University of London, UK. She is currently an associate professor with Southeast University. Her research interests lie in the areas of communication and signal processing, including ultra-low latency and high reliable communications, massive MIMO, and machine learning.

Kezhi Wang received the BEng and MEng degrees from Chongqing University, China, in 2008 and 2011, respectively. He received the PhD degree from University of Warwick, UK in 2015. He was a senior research officer in University of Essex, UK. Currently he is a senior lecturer with Department of Computer and Information Sciences at Northumbria University, UK. His research interests include wireless communications and machine learning.

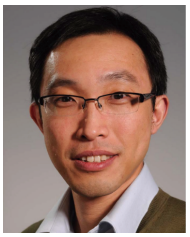

Kok Keong Chai received the BEng (Hons.), MSc, and PhD degrees, in 1998, 1999, and 2007, respectively. He joined the School of Electronic Engineering and Computer Science (EECS), Queen Mary University of London (QMUL), in August 2008. He is currently a reader of the Internet of Things, the Queen Mary Director of Joint Programme with Beijing University of Posts and Telecommunications (BUPT), and a Communication Systems Research Group Member, QMUL. His current research interests include sensing and prediction in distributed smart grid networks, smart energy charging schemes, applied blockchain technologies, dynamic resource management, wireless communications, and medium access control (MAC) for M2M communications and networks. He has authored more than 65 technical journals and conference papers in these areas.

Kai-Kit Wong received the BEng, MPhil, and PhD degrees in electrical and electronic engineering from Hong Kong University of Science and Technology, in 1996, 1998, and 2001, respectively. After graduation, he took up academic and research positions with the University of Hong Kong, Lucent Technologies, Bell-Labs, Holmdel, the Smart Antennas Research Group of Stanford University, and University of Hull, UK. He is currently the chair of wireless communications with the Department of Electronic and Electrical Engineering, University College London, UK. His current research interests include 5G and beyond mobile communications. He is a fellow of IET and IEEE. He was a co-recipient of the 2013 IEEE Signal Processing Letters Best Paper Award and the 2000 IEEE VTS Japan Chapter Award from the IEEE Vehicular Technology Conference, Japan, and a few other international best paper awards. He is also on the editorial board of several international journals. He has been the editor-in-chief of *IEEE Wireless Communications Letters* since 2020.